frontiers in Virology

ORIGINAL RESEARCH
published: 08 November 2021
doi: 10.3389/fviro.2021.690360

Complex Interactions Between Human Immunodeficiency Virus Type-1, Sex, and Osteopontin Influence Viral Replication and Leukocyte Proportions in Tissues

*Farina J. Mahmud[1], Elizabeth Greif[1], Thomas Boucher[1], Kelly A. Metcalf Pate[2], Claire Lyons[2], Bess Carlson[2] and Amanda M. Brown[1]**

[1] Department of Neurology, Johns Hopkins University School of Medicine, Baltimore, MD, United States, [2] Department of Molecular and Comparative Pathobiology, Johns Hopkins University School of Medicine, Baltimore, MD, United States

Evidence suggesting that HIV pathogenesis differs by sex, a variable known to influence the extent and breadth of immune responses in health and disease continues to accumulate. Host factors that promote or inhibit HIV replication may do so in a way that varies by sex. Prior studies using cultured human macrophages demonstrated that osteopontin (OPN)/secreted phosphoprotein-1 (SPP1) stimulates HIV replication. To test whether OPN has the same positive impact on virus replication at the level of tissues, we used a humanized mice model of low-level chronic HIV infection and in which OPN RNA and protein expression was inhibited with targeted aptamers. Interestingly, 4 months after infection when there were no significant differences in HIV viral load in plasma between groups however in contrast, in the spleen, lung, and liver the tissue burden of HIV RNA, as well as the proportion of leukocytes in female and male mice differed depending on whether OPN was expressed or not. The findings collectively demonstrate the potential for complex interactions between host factors like OPN and sex to influence different facets of HIV tissue-level pathogenesis.

Keywords: SPP-1, RNAscope, immunophenotyping, sex differences, viral RNA, humanized mice, HIV viral reservoir

OPEN ACCESS

Edited by:
Ravi Mahalingam,
University of Colorado, United States

Reviewed by:
Jay Rappaport,
Tulane University, United States
Charles Neff,
University of Colorado, United States

****Correspondence:***
Amanda M. Brown
abrown76@jhmi.edu

Specialty section:
This article was submitted to Modeling of Viral Replication and Pathogenesis, a section of the journal Frontiers in Virology

Received: *02 April 2021*
Accepted: *29 September 2021*
Published: *08 November 2021*

Citation:
Mahmud FJ, Greif E, Boucher T, Metcalf Pate KA, Lyons C, Carlson B and Brown AM (2021) Complex Interactions Between Human Immunodeficiency Virus Type-1, Sex, and Osteopontin Influence Viral Replication and Leukocyte Proportions in Tissues. Front. Virol. 1:690360. doi: 10.3389/fviro.2021.690360

INTRODUCTION

Human immunodeficiency virus type 1 (HIV-1) infection is managed with antiretroviral (ART) therapy while research toward a cure continues. HIV-1 disseminates rapidly into tissues forming sanctuaries and reservoirs which are harder to target (1–3). Replication-competent virus in such tissue reservoirs in tissues rebound into a full-fledged infection if ART is interrupted (4, 5). One of the significant challenges in HIV eradication strategies has been the absolute suppression of replication from tissue reservoirs (1, 4). Therefore, identifying and increasing our understanding of host cell genes that promote HIV replication in tissues would provide critical new knowledge.

Immune cells' ability to circulate and surveil tissues is potentially hijacked by HIV-1 to facilitate the formation of sanctuaries and reservoirs, suggesting a complex interaction between viral and host factors (6). Different anatomical and physiological properties of tissues also contribute to

reservoir formation and add another confounding dimension to eradicating reservoirs (6). HIV-1 infects $CD4^+$ T cells, monocytes, and tissue-resident macrophages throughout the body. The molecular mechanisms by which the virus establishes residency in these cells have pathways in common, while others are cell-autonomous (7). This reality highlights the heterogeneity of HIV reservoir formation and the challenge to eradication efforts.

There are also significant differences in HIV phenotypes and immune response between males and females, some of which have been attributed to socioeconomic and biological differences (8). Females account for almost half the population currently living with HIV, yet in early studies a consideration of sex differences in pathogenesis were rarely considered important in the design of effective treatment strategies (9). Plasma viral loads in females are lower than males, but females have a higher risk of acquisition (8, 10). Estradiol negatively impacts HIV replication, while testosterone has a positive association with plasma viral loads (11). Despite similar plasma viral loads, the burden of HIV in female lymph nodes was reported to be higher compared with similar tissue from males (8). Recent HIV vaccine trials have shown that females have enhanced interferon-stimulated gene expression and interferon-α (IFNα) response upon TLR7/9 activation and higher titers of neutralizing antibody than males suggesting enhanced immune responses (8, 11).

Moreover, these biological sequelae likely exacerbate the more robust activation of cytotoxic $CD8^+$ and higher $CD4^+$ loss seen in females vs. males (8, 11). Increased immune activation linked with HIV infection drives co-morbid conditions such as cardiovascular disease, cancer, and neurocognitive complications, which are augmented risk factors for females than males (12–14). Persistent immune activation and inflammation contribute to the maintenance and enhancement of viral replication by activating and stimulating the proliferation of memory $CD4^+$ T cells, which are highly susceptible to further infection (8, 15).

Osteopontin (OPN) is a multi-functional protein that is elevated during HIV infection, having both pro-survival as well as pro-and anti-inflammatory roles (16–18). HIV can use OPN to enhance replication, as demonstrated in cultured monocyte-derived macrophages via cell-cell fusion and through NF-κB signaling, which activates the HIV promoter (19). OPN can also function as a chemoattractant for monocytes and macrophages (20–22). Therefore, OPN's chemotactic, pro-survival, and viral replication promoting potential suggests that it may contribute *in vivo* to HIV pathogenesis and the recruitment and survival of infected immune cells in tissues.

In this study, we sought to understand whether inhibition of OPN RNA and protein expression in a humanized mice model for low-level chronic HIV infection can without antiretrovirals, reduce HIV reservoirs in the spleen, liver, and lung. The chimeric mouse model where immunocompromised NOD.Cg-PrkdcscidIL2rγtm1Wjl/SzJ (NSG) mice engrafted with human hematopoietic stem cells that develop a human immune system was used (23). Human T cells, monocytes, and macrophages were infected after intravenous challenge with HIV-1_{SF162}. Global inhibition of OPN expression at the RNA and protein level was achieved with oligonucleotide aptamers that block the interaction site of OPN with its receptors that, in turn, reduce signaling and gene expression through feedback suppression (24). At the study endpoint, viral loads in plasma were undetectable or very low and in the range of 2-3000 copies/ml.

Interestingly, using *in situ* hybridization to detect HIV-1 viral RNA, we found numerous foci of productively infected cells in the spleen and moderate levels in the lung and liver. Moreover, in the liver of mice with reduced OPN expression, there were fewer numbers of infected foci in the tissues of female compared to male mice. Reduction of OPN expression did not affect CD4:CD8 ratios, an indicator of immune dysfunction, however in all tissues examined, HIV infection was an additional source of variation that interacted in the liver with the variable sex (25–28). In the lungs, $CD14^+$ monocyte counts were significantly influenced by interactions with OPN and HIV infection. Interestingly, in the spleen, lung, and liver, there were significant interactions with HIV infection and $CD19^+$ B-cells counts, with an additional influence in the liver of male or female sex. Lastly, analyses of leukocyte proportions in each tissue revealed that OPN expression significantly influenced their relative levels.

MATERIALS AND METHODS

Humanized Mice Generation

All animal protocols and procedures were reviewed and approved by Johns Hopkins University Animal Care and Use Committee and Institutional Review Board (Protocol # MO17M12). The humanization protocol has been described previously (29), and the schematic of the study is illustrated in **Figure 1A**. NOD.Cg-Prkdc^{scid}IL2rγ^{tm1Wjl}/SzJ (NSG) (5–8 weeks old) mice were purchased from Jackson Laboratory for breeding colonies. Mice were housed and handled in pathogen-free environments. Newborn pups (P1–3) from breeders were irradiated at 100 cGy using Gamma Cell-40 Cesium Extractor (Theratronics) and injected intrahepatically with $1–2 \times 10^5$ cells of human fetal liver-derived CD34+ hematopoietic stem cells while under 2.5% isoflurane anesthesia. In mice, successful engraftment was identified 8 weeks post-engraftment from their peripheral blood with flow cytometry by staining and detecting human CD45 cells.

Mouse Groups

The humanized mice were separated and stratified into four groups of females and males either inhibited for OPN (treated with inhibitory aptamers that block OPN receptor signaling decreasing RNA and protein levels) or not (scrambled aptamers) and injected with HIV or buffer control [**Figure 1A**, (29)]. Mice were injected intravenously with HIV_{SF162} (1×10^5 tissue culture infectious doses/ml).

OPN Knockdown by Aptamer Treatments

HPLC purified Opn-R3 PTO (targets Opn) and Scrambled Opn-R3 aptamers were purchased from IBA Solutions for Life Sciences. Modifications to block endogenous nucleases were added to extend the half-life in blood circulation (ref 29). The sequence for Opn-R3-PTO was: 5′GGGAGGACGAUGCGG AUCAGCCAUGUUUACGUCACUCCU-3′ and for scrambled

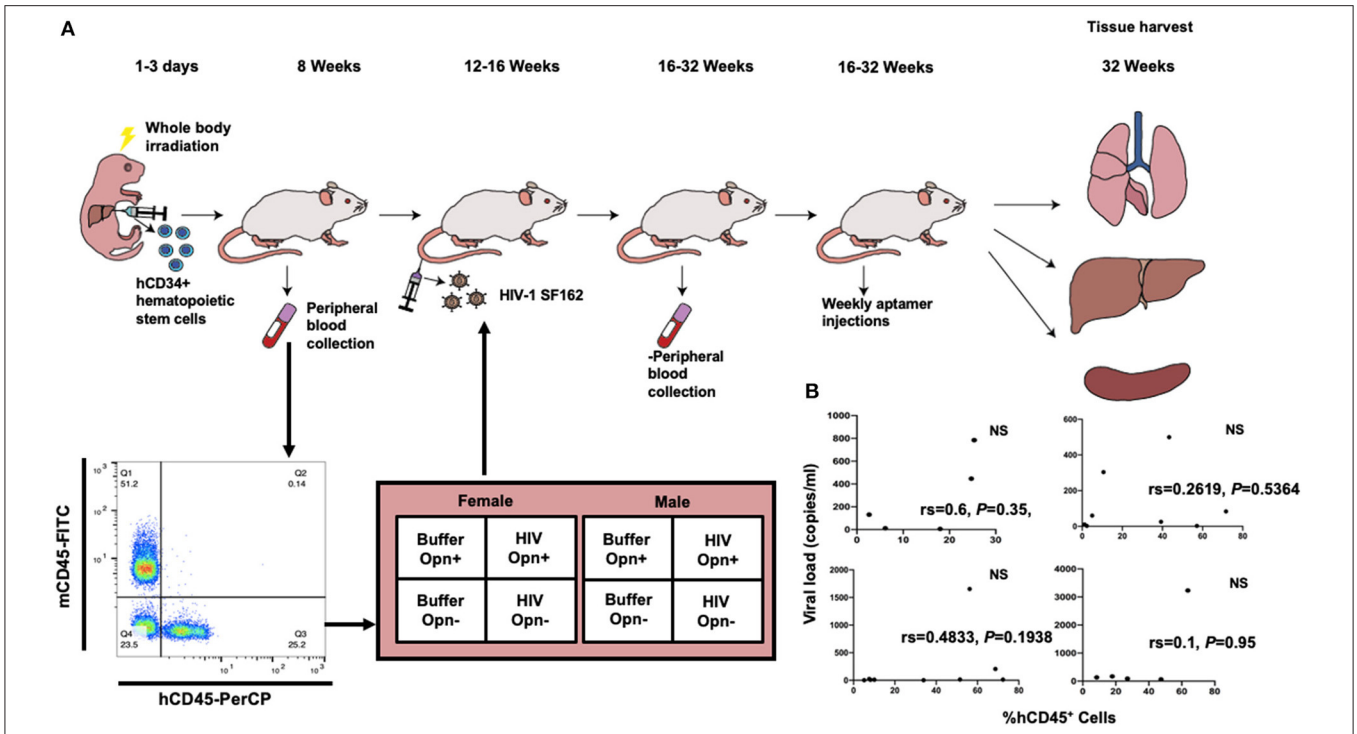

FIGURE 1 | Experimental design and correlation of viral loads with engraftment levels. **(A)** Illustrates the experimental design for the generation of hCD34+ humanized mice, HIV infection, groups implemented and the tissues harvested for the study. The time point for the tissue harvest reflects chronic infection. Representative flow cytometric dot plot of mouse blood-stained for human CD45-PerCP and mouse CD45-FITC used to identify successfully engrafted animals. The 2 × 2 design for female and male mice is indicated. **(B)** Correlation analyses between measured variables %hCD45^{+} cells (at time of engraftment) and viral loads (at study endpoint) for each mouse in the four HIV-infected groups. The Spearman coefficients (rs) indicated, while positive, did not reach significance ($P < 0.05$) in any of the groups. F-HIV-Opn+ $n = 5$, F-HIV-Opn– $n = 9$, M-HIV-Opn+ $n = 8$ and M-HIV-Opn– $n = 5$.

Opn-R3 was 5′-CGGCCACAGAAUGAAUCAUCGAUGUUG CAUAGUUG-3′. Aptamers were refolded into their tertiary structure before injection by heating them in folding buffer (1× PBS and 1 mM $MgCl_2$) at 93°C for 5 min. Seventy microliter of aptamers were intraperitoneally injected every week at a concentration of 1 mg/kg. Successful knockdown of Opn was confirmed by RT-PCR and IHC and reported previously (29).

Viral RNA RT-qPCR

Custom Taqman assay to determine HIV_{SF162} viral RNA as described previously (29). Briefly, RNA was extracted with QIAamp Viral RNA mini kit (Qiagen) and was reverse-transcribed to cDNA. HIV_{SF162} specific custom-designed primers forward: 5′CGA-ACC-CAG-ATT-GTAAGA-CT, reverse: 5′A CA-TGC-TGT-CAT-CAT-TTC-TTC and probe: 5′-FAM/A G-CAT-TAGG/ZEN/A-CCA-GCA-GCT-ACA-CT/3IABKFQ (Integrated DNA Technologies) and Taqman Fast Advanced Mastermix were used for cDNA amplification. Quantification was performed using a standard curve derived from a 10-fold dilution of HIV_{SF162} viral RNA.

Flow Cytometry for *ex vivo* Analysis of Peripheral Blood and Tissues

Peripheral blood (∼50 μl) taken by submandibular bleed was sampled at regular intervals. Tissues were evaluated at the study endpoint to validate and quantify human leukocytes by seven-color flow cytometry with a cocktail containing the following antibodies: human pan-CD45-Viogreen or PerCP (Miltenyi Biotec), 130-110-638, ThermoFisher (MHCD4531), CD3-PE (ThermoFisher, MHCD0304), CD4-Vioblue (Miltenyi Biotec, 130-113-219), CD8-APC-Vio770 (Miltenyi Biotec, 130-113-155), CD14-APC (BioLegend, 301808), CD19-FITC or PerCP (eBiosciences, 11-0199-42; BioLegend, 302228) and mouse CD45-FITC (eBiosciences, 11-0451-82). Peripheral blood was treated with ACK lysis buffer (ThermoFisher, A1049201) for red blood cell lysis, washed with HBSS (with cations, Gibco, 14025092) stained with the antibody cocktail. Cells were fixed with 1% Paraformaldehyde before flow cytometric acquisition. PBS perfused tissues were incubated in digestion media at 37°C for 45 min. They were then manually homogenized in FACS buffer (2% FBS, 1× PBS, and 0.5 mM EDTA) and strained through a 100 μM filter to obtain single-cell suspensions. The suspensions were subsequently centrifuged at 1,800 RPM, and the pellet was exposed to ACK lysis buffer for red blood cell lysis. The cells were then washed with HBSS (with cations) and split into two. One preparation was stained with an antibody cocktail, and the other was used as an unstained control. The cells were then fixed in 1% paraformaldehyde and introduced to MACsquant Analyzer 10 (Miltenyi Biotec) for flow cytometric acquisition.

RNA *in situ* Hybridization (RNAscope)

Chromogenic RNA *in situ* hybridization on HIV_{SF162} infected animals have been described previously (29). RNAscope kits and protocol were purchased from ACD Biosciences. HIV_{SF162} target probes were custom-designed to target Env-Nef sequences obtained from the accession number M65024.1 (2621–3701). Slides containing 10 μM sections of spleens, livers, and lungs were pretreated to retrieve their antigens according to the manufacturer's instructions. Custom probes were hybridized for 2 h in the HybEZ oven at 40°C. Amplification of target probe signal was performed the following day according to RNAscope 2.5 HD detection protocol. The fast red reagent was applied following amplification and developed for 10 min at room temperature. The nuclear stain was achieved with 30% Gill's Hematoxylin I (MilliporeSigma GHS132). Slides were mounted with Cytoseal 60 (#8310-4 Richard-Allan Scientific, ThermoFisher) and imaged on an ECHO Revolve microscope at 40× magnification.

Data Analysis and Statistics

RNAscope Images

Area covering the red staining (which depicts viral RNA) from the chromogenic images were quantified per image with FiJi Image J (NIH). The average area of a single RNA was quantified, and the total area per image was divided by this number to determine the number of viral RNA foci. The group means and standard deviations were combined using the average and square root of the variance approach. Particle analyses were performed with ordinary one-way ANOVA with Tukey's *post-hoc* test for multiple comparisons was performed to determine any differences between groups. Correlation analysis was performed to determine the relationship between independently measured values with reporting of the Spearman coefficient for non-parametric data and P-value <0.05 considered as significant (Graphpad Prism v8).

Flow Cytometry

FCS files from flow cytometry acquisition were analyzed with Flowjo v10. The data scanned for any anomalies using the flowAI plugin (30). Singlets were selected, followed by gating of cells from side-scatter vs. forward scatter. Human-specific leukocytes were selected by gating on hCD45 cells. Total T cells from cohort 2–4 were determined by gating on hCD3, and this was further used to characterize CD4 and CD8 populations. Monocytes and macrophages were evaluated using the CD14 marker, and absolute B cells were depicted using the CD19 marker. Dot plots were used when cells were abundant (T cells and B cells), and density plots were used to identify cell populations when their counts were lower (monocytes and macrophages). Three-way ANOVA analyses with a *post-hoc* test for normally distributed data by Tukey's and Kruskal-Wallis for non-parametric continuous data were employed to determine the variation in the immune cells due to Opn status, sex differences, and infection (Graphpad Prism v8). The mean and standard deviation (SD) is reported on all the figures with $^{*}P < 0.05$, $^{**}P < 0.01$, $^{***}P < 0.001$, and $^{****}P < 0.0001$.

Immunohistochemistry

Serial adjacent formalin-fixed paraffin-embedded tissue sections were treated and stained for with rabbit polyclonal antisera against human CD45 (HPA000440, SigmaAtlas) with 10 mM sodium citrate, 0.05% Tween-20, pH 6.0 antigen retrieval buffer, or human CD68 (bs-1432R, Bioss) with antigen retrieval buffer 10 mM Tris, 1 mM EDTA, 0.05% Tween-20 buffer, pH 9 as previously described (29).

RESULTS

In vivo Mouse Modeling of Low-Level Chronic HIV-1 Infection

Having identified OPN as an HIV-induced host cell protein that stimulates NF-κb mediated transcriptional activation, we utilized a model of low-level chronic HIV infection to assess OPN's role *in vivo* on HIV replication in plasma, spleen, lung, and liver of male and female NSG-hCD34+ humanized mice (**Figure 1A**). This model reflects many, but not all, aspects of viral pathogenesis and immunologic dysfunction observed in HIV infection (23, 31). The animals were stratified into four groups with varying degrees of human CD45 engraftment (**Table 1**). Successful inhibition of OPN was confirmed by RT-PCR and IHC and reported previously (29). For female HIV-infected mice irrespective of OPN levels, while a positive trend in the relationship between the percentage of $hCD45^{+}$ cells at initial infection and viral load at the study endpoint was observed [**Figure 1B**, Spearman coefficients (rs)], the correlations were not significant (**Figure 1B**, NS). These results suggest that the overall number of $hCD45^{+}$ cells at the time of engraftment did not drive plasma HIV copy number at the study endpoint. It is important here to highlight that the relationship between $hCD45^{+}$ cells and viral copy number is also expected to be influenced by the genetic background and susceptibility of the three human donors used for humanization (32, 33).

Variation in Levels of HIV RNA in the Spleen and Lungs in a Manner Dependent on Sex and OPN

More than 4 months after HIV infection, plasma viral load reached levels below 1,000 copies/ml in 25 out of 28 mice (**Table 1**). Tissues were harvested at a time point after HIV infection that represented 48–55 human years of chronic infection. This provided an opportunity to determine whether the spleen, a secondary lymphoid tissue, and the lung harbored productively infected cells and whether the formation of such sanctuaries differed in animals with reduced levels of OPN. Recent studies using models of humanized mice similar to that described herein have studied the establishment and kinetics of HIV sanctuaries, examining alterations in immune cell subsets, activation markers, and viral nucleic acids, but did not quantify vRNA at the single-cell level in tissues (31, 34, 35). RNA *in situ* hybridization was used to detect and enumerate HIV-1 load in the spleen, lung, and liver. Viral RNA was detected in the spleens of all the groups as strong and defined fast-red staining showing clusters of RNA coalesced together (**Figures 2A,B**,

TABLE 1 | Animal cohort information with details of treatment, sex, human CD45 cell engraftment levels at the time of infection and viral load at the study endpoint.

Cohort#	Animal ID	Treatment	Sex	%hCD45	Viral Load (copies/ml)
2	50	HIV-Opn+	F	2.65	130.37
2	51	HIV-Opn+	F	6.14	Undetectable
2	33	HIV-Opn+	F	24.74	446.28
2	34	HIV-Opn+	F	17.99	5.48
3	4	HIV-Opn+	F	25.37	784.78
3	5	HIV-Opn+	F	33.70	1059.43
2	18	HIV-Opn–	F	51.52	13.34
2	19	HIV-Opn–	F	72.34	12.63
2	20	HIV-Opn–	F	68.67	205.87
2	56	HIV-Opn–	F	6.18	Undetectable
2	57	HIV-Opn–	F	3.83	Undetectable
2	59	HIV-Opn–	F	1.82	2.97
2	60	HIV-Opn–	F	4.89	2.19
3	9	HIV-Opn–	F	4.97	9.16
3	11	HIV-Opn–	F	6.5	11.65
4	42	HIV-Opn–	F	56.20	1654.63
4	86	HIV-Opn–	F	7.6	24.30
2	7	HIV-Opn+	M	1.15	Undetectable
2	8	HIV-Opn+	M	2.3	2.43
2	23	HIV-Opn+	M	39.25	25.14
2	24	HIV-Opn+	M	71.67	83.48
2	26	HIV-Opn+	M	57.14	2.22
4	20	HIV-Opn+	M	43.31	499.56
4	30	HIV-Opn+	M	4.95	59.83
4	103	HIV-Opn+	M	10.6	303.82
2	35	HIV-Opn–	M	17.86	167.27
2	36	HIV-Opn–	M	8.45	131.41
2	37	HIV-Opn–	M	47.42	63.24
2	38	HIV-Opn–	M	27.05	89.82
3	1	HIV-Opn–	M	63.68	3232.07
2	42	Buffer-Opn+	F	10.2	
2	43	Buffer-Opn+	F	5.98	
2	44	Buffer-Opn+	F	10.0	
2	4	Buffer-Opn+	F	0.73	
2	84	Buffer-Opn+	F	0.5	
2	68	Buffer-Opn+	F	10.3	
2	39	Buffer-Opn–	F	8.52	
2	40	Buffer-Opn–	F	13.5	
2	41	Buffer-Opn–	F	5.93	
2	29	Buffer-Opn–	F	7.57	
2	30	Buffer-Opn–	F	34.7	
2	14	Buffer-Opn+	M	4.85	
2	16	Buffer-Opn+	M	4.04	
2	64	Buffer-Opn+	M	1.93	
2	65	Buffer-Opn+	M	2.49	
2	15	Buffer-Opn+	M	16.7	
2	52	Buffer-Opn–	M	2.63	
2	53	Buffer-Opn–	M	6.21	
2	55	Buffer-Opn–	M	2.08	
2	31	Buffer-Opn–	M	31.8	
3	2	Buffer-Opn–	M	32.4	

The table shows the cohort numbers, animal ID, group name, sex, engraftment levels (%hCD45), and viral loads in copies/mL from the study endpoint.

arrowheads, 40× magnification). Dense staining was detected in the white pulp, while sparse puncta were also observed in the red pulp, confirming the presence of HIV-infected lymphocytes and macrophages (**Figure 2A**, black and red arrowheads). Positive immunoreactivity with antisera against hCD45 to detect human leukocytes (black arrowheads) and hCD68 (red arrowheads, a marker for resident macrophages) further confirmed the presence of a subset of infected immune cells in these regions (**Figure 2A**). T-lymphocyte subsets were identified in the spleen by flow cytometry, suggesting the high likelihood that these cells harbor the majority of HIV RNA (**Figures 5D,E**). Some M-Opn+ spleens displayed viral RNA with a bursting pattern denoting possible cell lysis and spread (**Figure 2B**, third panel, arrows). The area covered by the fast red stain was measured and divided by the area of a single, representing one viral particle to determine the approximate total number of HIV viral particles per image (**Figure 2C**). Analyses of viral particle means and variation within groups followed by ordinary one-way ANOVA showed that the reduction of OPN expression significantly decreased HIV RNA burdens in the spleen, but only in female mice (**Figure 2D**, $P < 0.0001$). Significantly more HIV RNA was seen in the spleen of females expressing OPN compared to either male group (**Figure 2D**, $P < 0.0001$). A perfect positive correlation between plasma and tissue HIV RNA was found although it did not reach statistical significance (**Figure 2D**, Table rs = 1.0, $P = 0.0833$). At the study endpoint in mice with plasma loads below the limit of detection (**Table 1**), viral RNA puncta in tissues were found (**Figure 2C**, arrows). These findings suggest in the spleen a discordance between plasma viral load and the burden of splenic lymphocytes and macrophages persistently replicating HIV.

In the lungs, sparse HIV RNA puncta were detected in all infected groups (**Figure 3B**). H&E stains showed an influx of $hCD45^+$ cells from blood vessels into the lung parenchyma (**Figure 3A**, black arrows). Viral RNA was present in these recent migrating cells (**Figure 3A**, black arrowheads) and cells near (interstitial macrophages) or lining lung alveoli (alveolar macrophages) (**Figure 3B**, black arrowheads). A small number of cells were also found to be hCD68 positive and HIV-infected (**Figure 3A**, red arrowheads).

Overall, HIV RNA levels were 10-fold lower in the lung than in the spleen (**Figure 2D** vs. **Figure 3D**). In the lung, HIV RNA levels were 2-fold higher in females with reduced OPN than those with regular OPN expression (**Figure 3D**, $P < 0.0001$). The reverse relationship was seen in male lungs, where the number of HIV RNA particles was significantly higher with OPN normal expression (**Figure 3D**, $P < 0.002$). We also noted viral RNA puncta in the lungs of mice with undetectable viral RNA in their plasma at the study endpoint (**Table 1**, **Figure 3C**, arrows).

Higher Levels of HIV RNA Were Detected in the Liver of Male Mice Expressing OPN

A large influx of hCD45+ cells into the tissue parenchyma was observed in the liver (**Figure 4A**, arrows). Viral RNA was present in a subset of these cells (**Figures 4A,B**, black arrowheads). Human $CD68^+$ macrophages were found within and adjacent

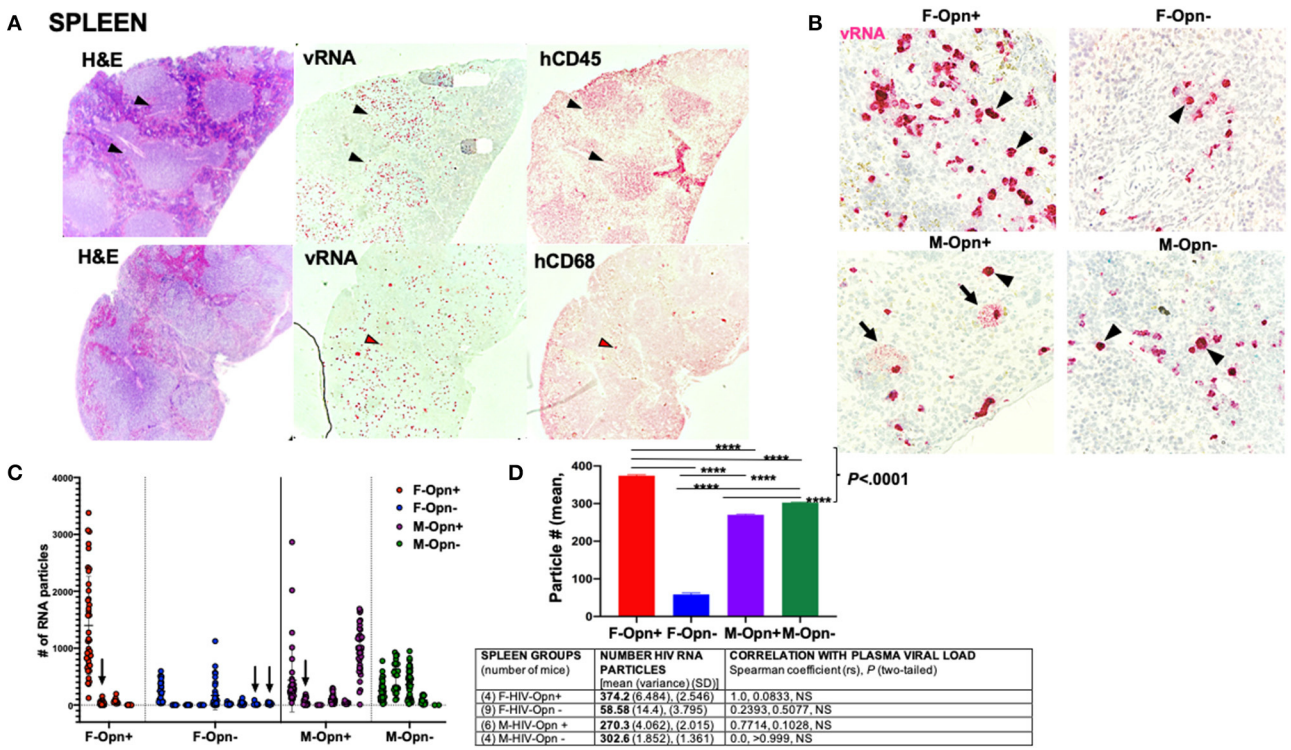

SPLEEN GROUPS (number of mice)	NUMBER HIV RNA PARTICLES [mean (variance) (SD)]	CORRELATION WITH PLASMA VIRAL LOAD Spearman coefficient (rs), *P* (two-tailed)
(4) F-HIV-Opn+	**374.2** (6.484), (2.546)	1.0, 0.0833, NS
(9) F-HIV-Opn -	**58.58** (14.4), (3.795)	0.2393, 0.5077, NS
(6) M-HIV-Opn +	**270.3** (4.062), (2.015)	0.7714, 0.1028, NS
(4) M-HIV-Opn -	**302.6** (1.852), (1.361)	0.0, >0.999, NS

FIGURE 2 | Spleen viral load and correlation with plasma burden. **(A)** Shows representative images infected spleens with viral RNA concentrated in the white pulp positive for hCD45 (black arrowheads) and red pulp in cells positive for hCD68 (red arrowheads). **(B)** Shows 40× images of spleens stained for their viral RNA (black arrowheads). Bursting pattern of viral dissemination observed in the males (black arrows). **(C)** Quantification of the viral RNA from the spleen is shown. Individual points and mean ± SD are displayed. Arrows show animals with undetectable plasma viral loads but had low levels of viral RNA present in their spleen. **(D)** Group means, variance and SD, and Spearman correlation coefficient with significance $P < 0.05$ are given in the Table.

to blood vessels with a subset showing positivity for viral RNA (**Figure 4A**, red arrowheads). Three males exhibiting very high plasma loads had giant clusters of viral RNA surrounded by many hematoxylin positive nuclei, a pattern not observed in any female group (**Figure 4B**, arrows). While no differences in HIV RNA burden in the two female mice groups were seen, males expressing normal levels of OPN had the highest levels of viral RNA particles (**Figure 4D**, $P < 0.0001$). Moreover, there was a significant positive correlation between the plasma and liver viral loads in infected males expressing OPN (**Figure 4D**, Table, rs = 0.893, $P = 0.0417$).

Variation in CD4$^+$ Cell Levels and CD4:CD8 Ratios Are Not Modulated by OPN Expression

In addition to lowering viral loads, ART normalizes CD4:CD8 ratios and reverses some of the HIV-induced T cell dysfunction when administered during the acute phase of infection (36–38). OPN through a NF-κB signaling pathway enhances HIV replication in HIV target cells (19, 39). ART was not used in this study, but rather we tested the hypothesis that inhibiting OPN expression would serve to decrease HIV replication and thereby spare CD4$^+$ T-cell depletion. Human CD4 and CD8 T cell (hCD4, hCD8) population levels found in the spleen, lung and liver where quantified by flow cytometric analyses on freshly prepared single-cell suspensions generated from PBS-perfused tissues. A gating strategy based on human CD45 (hCD45) lymphocytes was used to analyze human specific leukocytes in the spleen (**Supplementary Figure 1**). For all tissues there were no significant between group differences (**Figures 5–7A–C**, NS). However, three-way ANOVA analyses with post-test for normally distributed data by Tukey's and Kruskal-Wallis for non-parametric continuous data were used to enumerate potential variation and interaction between sex, OPN status and HIV infection. In the spleen, a decrease in total T cells (hCD3$^+$) in both female infected groups was observed (**Figure 5D**, F vs. M × HIV vs. Buffer $P = 0.0384$; 9.5% of the total variance); hCD3$^+$ mean (SD): F-Opn+, $n = 7$, 28.78 (16.13); F-Opn–, $n = 7$, 38.23 (12.34); HIV-F-Opn+, $n = 5$, 11.19 (6.922); HIV-F-Opn–, $n = 6$, 27.83 (13.8); M-Opn+, $n = 5$, 33.48 (29.36); M-Opn–, $n = 5$, 29.6 (29.05); HIV-M-Opn+, $n = 7$, 42.14 (34.82); HIV-M-Opn–, $n = 5$, 47.54 (4.233). A highly significant interaction with HIV and the number of hCD4$^+$ cells was seen in all HIV-infected groups compared to uninfected mice, although the decrease in female infected mice was more intense [**Figure 5E**, HIV vs. Buffer $P = 0.0020$; 19.7% of the total variance; hCD4$^+$ mean (SD): F-Opn+, $n = 7$, 56.54 (15.76); F-Opn–, $n = 7$, 55.78 (12.17);

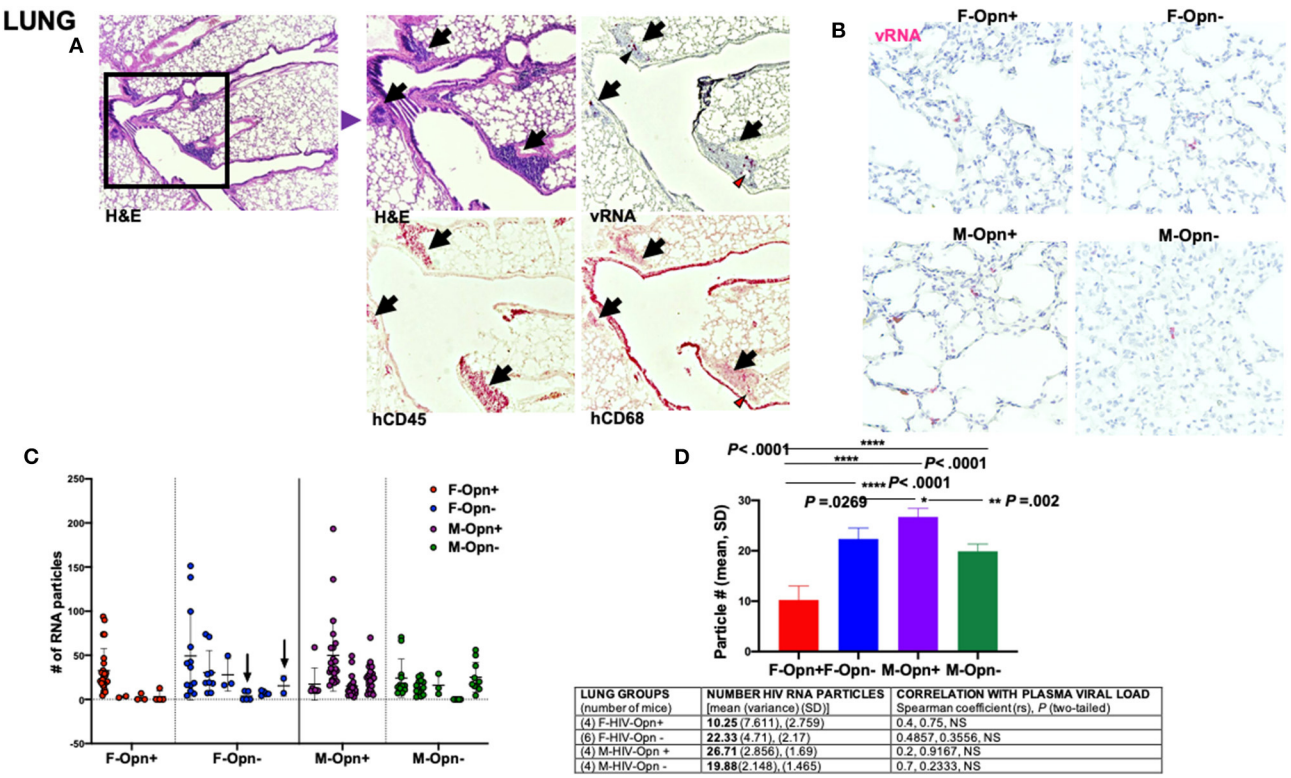

LUNG GROUPS (number of mice)	NUMBER HIV RNA PARTICLES [mean (variance) (SD)]	CORRELATION WITH PLASMA VIRAL LOAD Spearman coefficient (rs), *P* (two-tailed)
(4) F-HIV-Opn+	**10.25** (7.611), (2.759)	0.4, 0.75, NS
(6) F-HIV-Opn -	**22.33** (4.71), (2.17)	0.4857, 0.3556, NS
(4) M-HIV-Opn +	**26.71** (2.856), (1.69)	0.2, 0.9167, NS
(4) M-HIV-Opn -	**19.88**(2.148), (1.465)	0.7, 0.2333, NS

FIGURE 3 | Lung viral load and correlation with plasma burden. **(A)** Shows representative images of infected lungs with a large infiltrate of cells positive for hCD45 (black arrows) and containing viral RNA (black arrowheads). Some cells adjacent to the blood vessels were positive for hCD68 and infected (red arrowheads). **(B)** 40× images of lungs stained for HIV viral RNA (red). **(C)** Quantification of the viral RNA from the lung is shown. Individual points and mean ± SD are displayed. Arrows show animals with undetectable plasma viral loads but had low levels of viral RNA present in their lung. **(D)** Group means, variance and SD, and Spearman correlation coefficient with significance $P < 0.05$ are given in the Table.

HIV-F-Opn+ ($n = 5$, 19.93 (7.274); HIV-F-Opn–, $n = 5$, 27.19 (16.85); M-Opn+, $n = 5$, 33.70 (24.39); M-Opn–, $n = 5$, 51.7 (33.85); HIV-M-Opn+, $n = 7$, 32.96 (17.78); HIV-M-Opn–, $n = 5$, 40.84 (11.02)]. Indeed, this difference in $hCD4^+$ cells was also driven by sex (**Figure 5B**, F vs. M × HIV vs. Buffer $P = 0.0256$; 9.59% of the total variance). An increase in cytotoxic $hCD8^+$ T cells, which led to a corresponding decrease in the hCD4:hCD8 was seen in all HIV-infected groups irrespective of OPN expression (**Figure 5C**, HIV vs. Buffer $P = 0.0030$, 18.6% of the total variance in $hCD8^+$; **Figure 5E**, $P = 0.0171$, HIV, 12.88% of the total variance in hCD4:hCD8 ratio; $CD8^+$ mean (SD): F-Opn+ ($n = 7$, 56.54 (15.76); F-Opn–, $n = 7$, 55.78 (12.17); HIV-F-Opn+ ($n = 5$, 19.93 (7.274); HIV-F-Opn–, $n = 6$, 27.19 (16.85); M-Opn+, $n = 5$, 33.70 (24.39); M-Opn–, $n = 5$, 51.7 (33.85); HIV-M-Opn+, $n = 7$, 32.96 (17.78); HIV-M-Opn–, $n = 5$, 40.84 (11.02); CD4:CD8 ratio mean (SD): F-Opn+ ($n = 7$, 0.3091 (0.3248); F-Opn–, $n = 7$, 0.1634 (0.4033); HIV-F-Opn+ ($n = 5$, −0.0418 (0.5053); HIV-F-Opn–, $n = 6$, 0.1373 (0.6597); M-Opn+, $n = 5$, 0.1917 (0.213); M-Opn–, $n = 5$, 0.5995 (0.3399); HIV-M-Opn+, $n = 6$, −0.02613 (0.3338); HIV-M-Opn–, $n = 5$, −0.00183 (0.1959). These results suggest that in the spleen, disruption of OPN expression had no significant additive effect on HIV-induced dysregulation of $hCD4^+$ and $hCD8^+$ T cell numbers. Interestingly, female, as compared to male mice, tended to suffer $hCD4^+$ loss to a greater extent.

Analyses of the lungs revealed a decrease in total $hCD3^+$ cells that was associated with HIV infection [**Figure 6A**, HIV vs. Buffer $P = 0.0110$; 12.66% of the total variance; hCD3 mean (SD): F-Opn+, $n = 5$, 22.3 (6.531); F-Opn–, $n = 10$, 37.63 (22.18); HIV-F-Opn+, $n = 7$, 55.57 (17.95); HIV-F-Opn–, $n = 6$, 66.23 (10.05); M-Opn+, $n = 3$, 56 (39.32); M-Opn–, $n = 4$, 56.6 (35.49); HIV-M-Opn+, $n = 8$, 39.84 (24.64); HIV-M-Opn–, $n = 5$, 59.5 (26.36)]. As expected, viral infection was also associated with the reduction in hCD4 cells in all the infected compared to uninfected groups accounting for 17.86% of the total variance [**Figures 6B,C,E**, HIV vs. Buffer $P = 0.0074$; hCD4 mean (SD): F-Opn+, $n = 4$, 60.95 (15.3); F-Opn–, $n = 4$, 77.1 (11.48); HIV-F-Opn+, $n = 6$, 65.03 (15.45); HIV-F-Opn–, $n = 7$, 44.2 (22.28); M-Opn+, $n = 3$, 75.6 (26.75); M-Opn–, $n = 4$, 78.37 (8.33); HIV-M-Opn+, $n = 5$, 60.26 (19.95); HIV-M-Opn–, $n = 5$, 54.08 (15.69)]. A highly significant interaction between $hCD8^+$ levels with HIV infection found [**Figure 6C**, HIV vs. Buffer $P = 0.0009$; 18.4% of the total variance; hCD8 mean (SD):

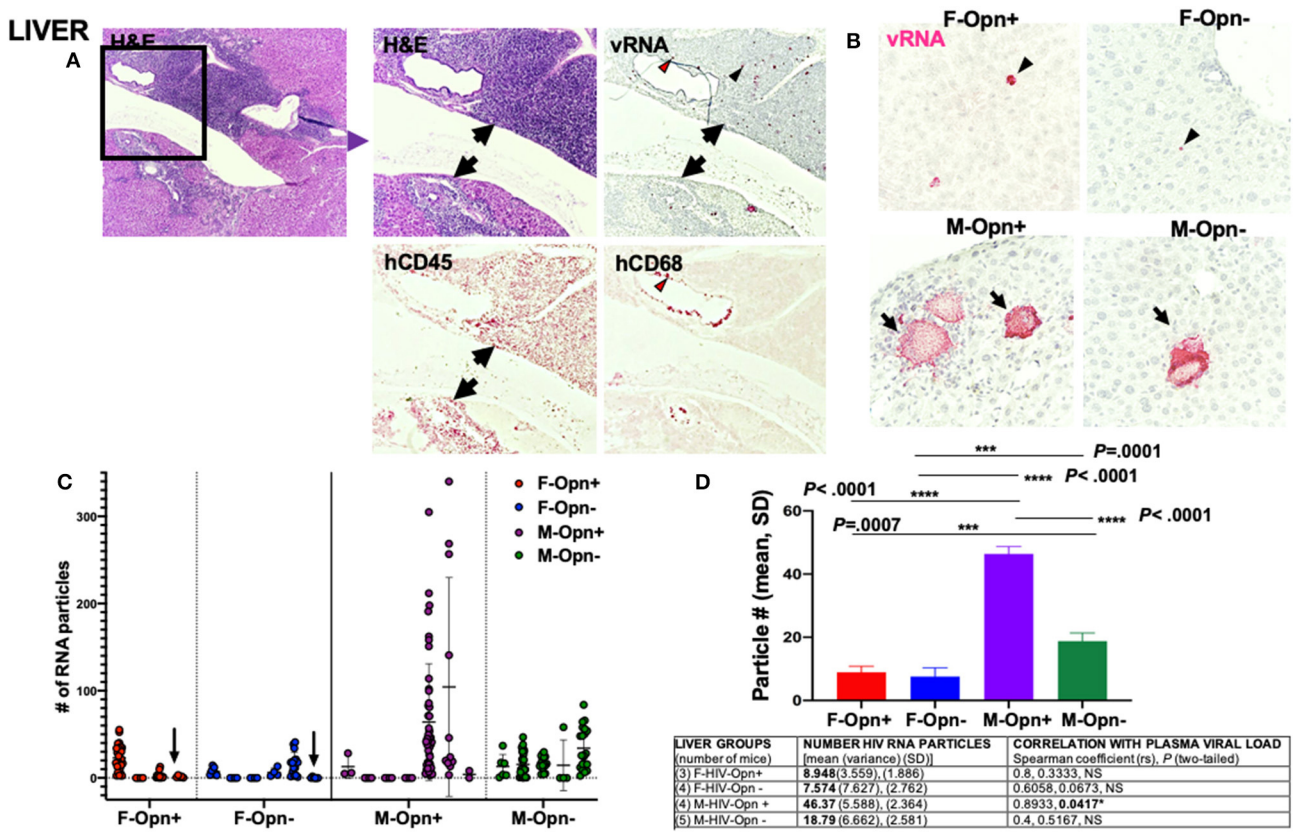

LIVER GROUPS (number of mice)	NUMBER HIV RNA PARTICLES [mean (variance) (SD)]	CORRELATION WITH PLASMA VIRAL LOAD Spearman coefficient (rs), *P* (two-tailed)
(3) F-HIV-Opn+	**8.948** (3.559), (1.886)	0.8, 0.3333, NS
(4) F-HIV-Opn -	**7.574** (7.627), (2.762)	0.6058, 0.0673, NS
(4) M-HIV-Opn +	**46.37** (5.588), (2.364)	0.8933, **0.0417***
(5) M-HIV-Opn -	**18.79** (6.662), (2.581)	0.4, 0.5167, NS

FIGURE 4 | Liver viral load and correlation with plasma burden. **(A)** Shows representative images of infected liver with a large infiltrate of cells positive for hCD45 (black arrows) and containing viral RNA (black arrowheads). Some cells adjacent to the blood vessels were positive for hCD68 and infected (red arrowheads). **(B)** 40× images of liver stained for HIV viral RNA (red). Giant clusters of viral RNA surrounded by many hematoxylin positive nuclei in male mice's liver. **(C)** Quantification of the viral RNA from the liver is shown. Individual points and mean±SD are displayed. Arrows show animals with undetectable plasma viral loads but had low viral RNA levels present in their liver. **(D)** Group means, variance and SD, and Spearman correlation coefficient with significance $P < 0.05$ are given in the Table.

F-Opn+, $n = 7$, 22.15 (11.44); F-Opn–, $n = 6$, 15.97 (9.576); HIV-F-Opn+, $n = 6$, 18.92 (16.37); HIV-F-Opn–, $n = 10$, 41.35 (18.24); M-Opn+, $n = 3$, 10.48 (12.63); M-Opn–, $n = 4$, 5.878 (5.467); HIV-M-Opn+, $n = 8$, 30.47 (17.95); HIV-M-Opn–, $n = 5$, 26.14 (7.667)]. There were no significant between group differences in hCD4:hCD8 ratios however, HIV infection and sex contributed individually and in combination to the variation [**Figure 6E**, HIV, $P = 0.0069$, Sex, $P = 0.0146$, HIV × Sex, $P = 0.017$; hCD4:hCD8 ratio mean (SD): F-Opn+ ($n = 7$, 0.1306 (0.6409); F-Opn–, $n = 6$, 0.4438 (0.8502); HIV-F-Opn+ ($n = 5$, −0.5591 (0.5421); HIV-F-Opn–, $n = 10$, −0.1261 (0.5553); M-Opn+, $n = 3$, 1.115 (0.8598); M-Opn–, $n = 3$, 1.438 (0.4254); HIV-M-Opn+, $n = 8$, 0.1380 (0.6345); HIV-M-Opn–, $n = 5$, 0.3201 (0.2594)].

In the liver, there were no significant between- or intra-group differences in hCD3 and hCD8 cell numbers [**Figures 7A–C**, ns; CD3 mean (SD): F-Opn+ ($n = 7$, 59.36 (20.72); F-Opn–, $n = 7$, 66.44 (16.05); HIV-F-Opn+ ($n = 6$, 58.73 (31.18); HIV-F-Opn–, $n = 9$, 54.04 (27.98); M-Opn+, $n = 3$, 68.1 (37.85); M-Opn–, $n = 5$, 62.86 (36.96); HIV-M-Opn+, $n = 8$, 66.02 (32.42); HIV-M-Opn–, $n = 5$, 81.46 (24.75); CD8 mean (SD): F-Opn+ ($n = 7$, 16.21 (9.457); F-Opn–, $n = 7$, 25.13 (10.44); HIV-F-Opn+ ($n = 6$, 18 (14.64); HIV-F-Opn–, $n = 9$, 31.38 (9.106); M-Opn+, $n = 3$, 18.87 (22.59); M-Opn–, $n = 5$, 12.83 (16); HIV-M-Opn+, $n = 7$, 18.66 (12.52); HIV-M-Opn–, $n = 5$, 25.8 (10.69)]. In contrast, intra-group decreases in hCD4 cells that was associated with HIV infection was detected [**Figure 7D**, HIV vs. Buffer $P = 0.0043$; CD4 mean (SD): F-Opn+ ($n = 4$, 46.82 (16.42); F-Opn–, $n = 5$, 43.24 (13.8); HIV-F-Opn+ ($n = 6$, 31.67 (13.2); HIV-F-Opn–, $n = 9$, 21.52 (10.98); M-Opn+, $n = 3$, 54.7 (13.34); M-Opn–, $n = 5$, 43.86 (18.96); HIV-M-Opn+, $n = 8$, 42.77 (21.36); HIV-M-Opn–, $n = 5$, 33.7 (9.30)]. There was a modest trend of higher CD4:CD8 particularly in an interaction with viral infection in male mice [**Figure 7E**, sex as a source of variation, 11.63%, $P = 0.0201$; CD4:CD8 ratio mean (SD): F-Opn+ ($n = 6$, −0.1122 (0.4398); F-Opn–, $n = 7$, −0.005514 (0.4228); HIV-F-Opn+ ($n = 4$, 0.2653 (0.2759); HIV-F-Opn–, $n = 9$, −0.2249 (0.3541); M-Opn+, $n = 2$, 0.2992 (0.3606); M-Opn–, $n = 4$, 0.5720 (0.6067); HIV-M-Opn+, $n = 5$, 0.1770 (0.5841); HIV-M-Opn–, $n = 6$, 0.4294 (0.7491)]. Collectively, these results suggest moderate to

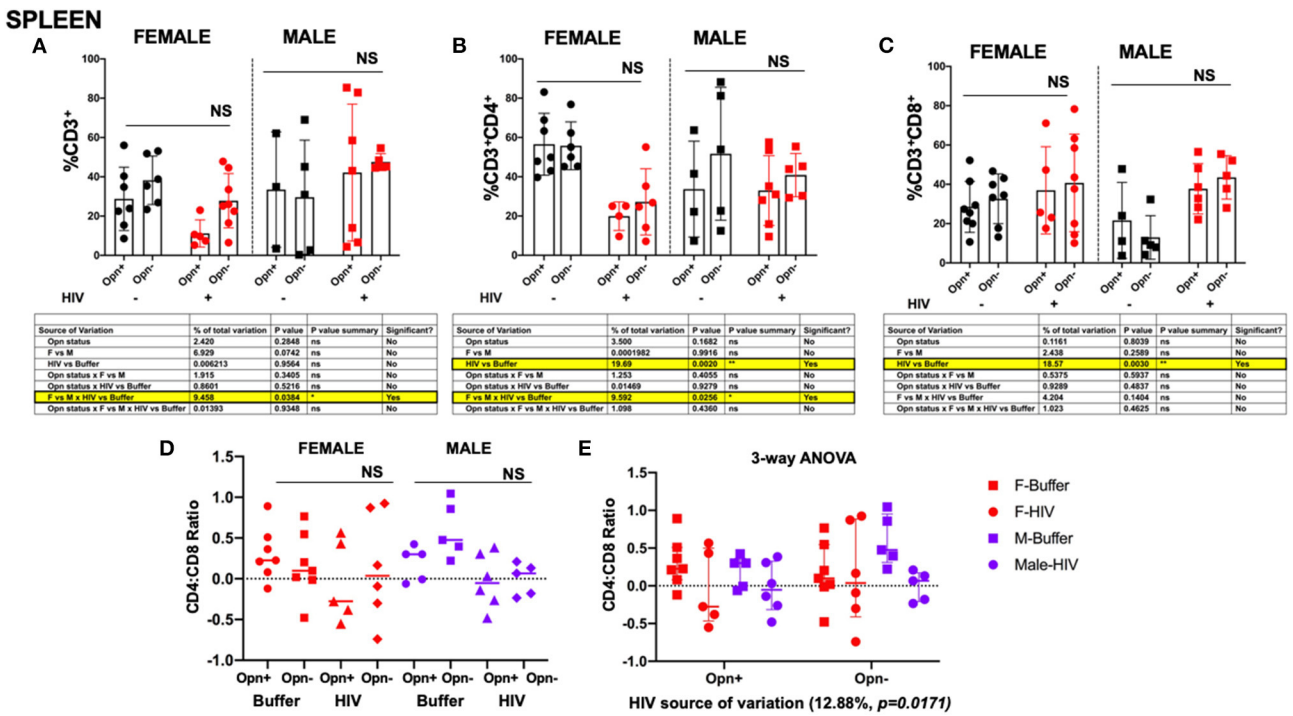

FIGURE 5 | Flow cytometric analyses of T cell subsets in the spleen. **(A)** Shows the percentage of CD3+, **(B)** percentage of CD4+ and **(C)**, percentage of CD8+ in the spleen. Individual points and mean±SD are displayed. Three-way ANOVA, with Tukey's *post-hoc* for normally distributed data to determine the variation in the immune cells due to Opn status, sex differences, and infection; results are displayed below the bar charts with significant results highlighted. **(D,E)** CD4:CD8 ratio analyses were performed with three-way ANOVA for non-parametric continuous data and *post-hoc* test by Kruskal-Wallis to determine the variation in the immune cells due to Opn status, sex differences, and infection. $^{*}P < 0.05$, $^{**}P < 0.01$, $^{***}P < 0.001$, and $^{****}P < 0.0001$. **Infected**: F-HIV-Opn+ $n = 5$, F-HIV-Opn–$n = 6$, M-HIV-Opn+ $n = 7$ and M-HIV-Opn– $n = 5$. **Uninfected**: F-Opn+ $n = 7$, F-Opn– $n = 7$, M-Opn+ $n = 5$ and M-Opn– $n = 5$.

strong influences of HIV infection and/or sex in the tissue levels of T-lymphocytes in the spleen, lung and liver in a model of low-level chronic infection of NSG-hCD34 humanized mice.

Both HIV Infection and OPN Expression Influence the Number of CD14^{+} Monocytes in the Lungs, but Not in the Spleen or Liver

Monocyte trafficking into tissues is increased in HIV-infected individuals and plays a role in promoting inflammatory sequelae and enhancing the HIV reservoir (40). Monocyte numbers in the spleen, lung, and liver were assessed by FACS using antisera against hCD14, a marker for the lipoprotein receptor (LPS) responsible in concert with toll-like receptor signaling, for potentiating inflammatory responses (40, 41). The gating strategy for spleen, lung and liver is shown in **Supplementary Figure 4**. Three-way ANOVA (non-parametric, spleen and lung; parametric, liver) of single-cell suspensions of the spleen demonstrated that there were no differences in the hCD14^{+} levels in the spleen between groups, but most of the females from every group had very low counts compared to males [**Figures 8A–C**; CD14 mean (SD): F-Opn+ ($n = 5$, 357.2 (194.7); F-Opn–, $n = 5$, 812.6 (1,168); HIV-F-Opn+ ($n = 4$, 223.7 (170.1); HIV-F-Opn–, $n = 5$, 181.2 (73.5); M-Opn+, $n = 4$, 702.2 (1,055); M-Opn–, $n = 5$, 1142.6 (1859.12); HIV-M-Opn+, $n = 5$, 702.2 (1,055); HIV-M-Opn–, $n = 4$, 886.5 (795.8)]

In contrast, in the lung for both female and male mice, interactions between HIV infection and OPN expression impacted the variation in CD14 counts. Higher numbers of hCD14^{+} cells were seen in both infected and uninfected groups when compared to animals expressing OPN [**Figures 8A–C**, HIV infection, 14.17% of the total variation, $P = 0.0304$; OPN status 12.96% of the variation, $P = 0.0377$; hCD14 mean (SD): F-Opn+, $n = 4$, 296.5 (171.8); F-Opn–, $n = 4$, 520.2 (574.7); HIV-F-Opn+, $n = 4$, 75.25 (76.53); HIV-F-Opn–, $n = 5$, 214.8 (215.1); M-Opn+, $n = 3$, 211.7 (174.8); M-Opn–, $n = 4$, 687.5 (507.5); HIV-M-Opn+, $n = 5$, 152.6 (121.3); HIV-M-Opn–, $n = 4$, 271.5 (275.4)]. Similar analyses of cells in the liver did not reveal any differences due to infection, sex or OPN status (**Figure 8C**).

These results indicate that irrespective of virus replication, OPN expression can impact monocyte numbers in the lungs. Chronic HIV infection independently reduces the number of monocytes in the lungs, while reducing OPN increases monocyte trafficking to this tissue in a manner independent of HIV infection.

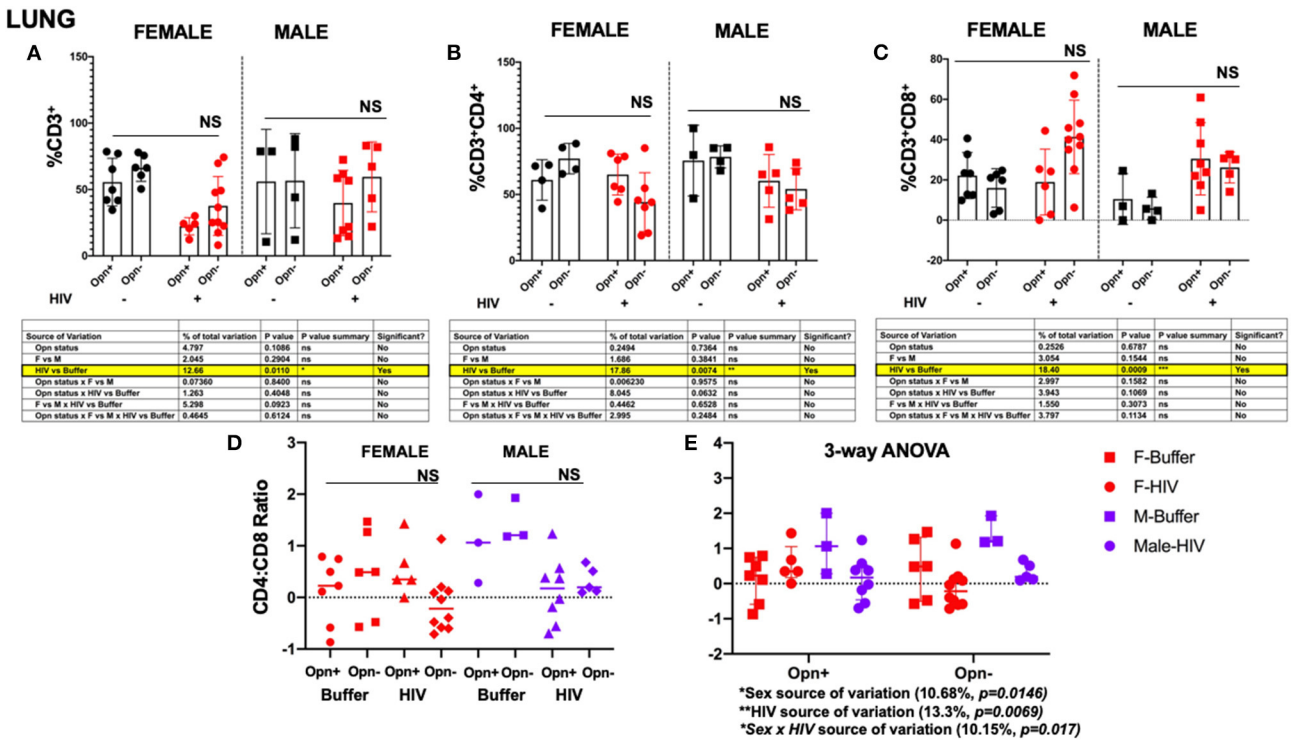

Source of Variation	% of total variation	P value	P value summary	Significant?
Opn status	4.797	0.1086	ns	No
F vs M	2.045	0.2904	ns	No
HIV vs Buffer	12.66	0.0110	*	Yes
Opn status x F vs M	0.07360	0.8400	ns	No
Opn status x HIV vs Buffer	1.263	0.4048	ns	No
F vs M x HIV vs Buffer	5.298	0.0923	ns	No
Opn status x F vs M x HIV vs Buffer	0.4645	0.6124	ns	No

Source of Variation	% of total variation	P value	P value summary	Significant?
Opn status	0.2494	0.7364	ns	No
F vs M	1.686	0.3841	ns	No
HIV vs Buffer	17.86	0.0074	**	Yes
Opn status x F vs M	0.006230	0.9575	ns	No
Opn status x HIV vs Buffer	8.045	0.0632	ns	No
F vs M x HIV vs Buffer	0.4462	0.6528	ns	No
Opn status x F vs M x HIV vs Buffer	2.995	0.2484	ns	No

Source of Variation	% of total variation	P value	P value summary	Significant?
Opn status	0.2526	0.6787	ns	No
F vs M	3.054	0.1544	ns	No
HIV vs Buffer	18.40	0.0009	***	Yes
Opn status x F vs M	2.997	0.1582	ns	No
Opn status x HIV vs Buffer	3.943	0.1069	ns	No
F vs M x HIV vs Buffer	1.550	0.3073	ns	No
Opn status x F vs M x HIV vs Buffer	3.797	0.1134	ns	No

FIGURE 6 | Flow cytometric analyses of T cell subsets in the lung. **(A)** Shows the percentage of CD3+ **(B)** percentage of CD4+ and **(C)**, percentage of CD8+. Individual points and mean ± SD are displayed. Three-way ANOVA, with Tukey's *post-hoc* for normally distributed data to determine the variation in the immune cells due to Opn status, sex differences, and infection; results are displayed below the bar charts with significant results highlighted. **(D,E)** CD4:CD8 ratio analyses were performed with three-way ANOVA for non-parametric continuous data and *post-hoc* test by Kruskal-Wallis to determine the variation in the immune cells due to Opn status, sex differences, and infection. $^{*}P < 0.05$, $^{**}P < 0.01$, $^{***}P < 0.001$, and $^{****}P < 0.0001$. **Infected**: F-HIV-Opn+ $n = 6$, F-HIV-Opn– $n = 10$, M-HIV-Opn+ $n = 8$ and M-HIV-Opn– $n = 5$. **Uninfected**: F-Opn+ $n = 7$, F-Opn– $n = 6$, M-Opn+ $n = 3$ and M-Opn– $n = 4$.

CD19^{+} B Cell Loss Observed in Spleen, Lungs, and Liver of Infected Animals Is Driven by HIV-1 Infection

The absolute number of B cells in plasma usually declines in response to acute or chronic HIV replication (25, 42). Therefore, we evaluated whether human B cell numbers in spleen, lung and liver followed a similar pattern in our HIV-infected humanized mice and whether OPN expression had any impact on this response. The FACS gating strategy for spleen, lung and liver is provided in **Supplementary Figure 5**. Analysis of the spleen, lung and liver revealed significant intra-group decreases in CD19^{+} cells in HIV-infected mice irrespective of OPN status [**Figures 9A–C**; spleen: HIV 12.72% of the total variance, $P = 0.0362$; lung: HIV 21.92% of the total variance $P = 0.0068$; liver: HIV 15.69% of the total variance $P = 0.0056$; spleen CD19 mean (SD): F-Opn+, $n = 5$, 6664 (6,642); F-Opn–, $n = 5$, 3927 (4,153); HIV-F-Opn+, $n = 4$, 2455 (4,484); HIV-F-Opn–, $n = 5$, 771 (697.3); M-Opn+, $n = 4$, 2256 (2,185); M-Opn–, $n = 5$, 4739 (5,648); HIV-M-Opn+, $n = 5$, 991.2 (1,201); HIV-M-Opn–, $n = 4$, 1,845 (526.2); lung CD19 mean (SD): F-Opn+, $n = 4$, 319.5 (290.6); F-Opn–, $n = 4$, 526.5 (352.9); HIV-F-Opn+ ($n = 4$, 100.5 (128.4); HIV-F-Opn–, $n = 5$, 73.6 (66.57); M-Opn+, $n = 3$, 126.7 (97.52); M-Opn–, $n = 4$, 512.2 (605); HIV-M-Opn+, $n = 5$, 107.4 (108.7); HIV-M-Opn–, $n = 4$, 71.25 (51.34); liver CD19 mean (SD): F-Opn+, $n = 3$, 73.33 (83.72); F-Opn–, $n = 5$, 234.8 (144.4); HIV-F-Opn+, $n = 4$, 30 (27.31); HIV-F-Opn–, $n = 5$, 29.25 (32.23); M-Opn+, $n = 3$, 30.67 (25.54); M-Opn–, $n = 4$, 68.5 (69.66); HIV-M-Opn+, $n = 5$, 21.8 (19.9); HIV-M-Opn–, $n = 4$, 15.5 (15.97)]. Additionally, in the liver uninfected females had higher levels of B cells than males particularly between the groups in which OPN expression was inhibited (Figure 9M, sex 8.662% of the total variance, $P = 0.033$).

Proportional Differences of CD3^{+} T Cells, CD19^{+} B Cells, and CD14^{+} Monocytes in Mice With Low Levels of OPN Expression

OPN can function as a chemoattractant facilitating the recruitment of leukocytes into tissues and promoting cell survival (17, 18, 20). In this scenario, knockdown of chemotactic and pro-survival signaling through OPN expression interference would be expected to reduce any increased immune cell influx stimulated by HIV infection. Therefore, we hypothesized that the percent frequency of each subpopulation of leukocytes might be

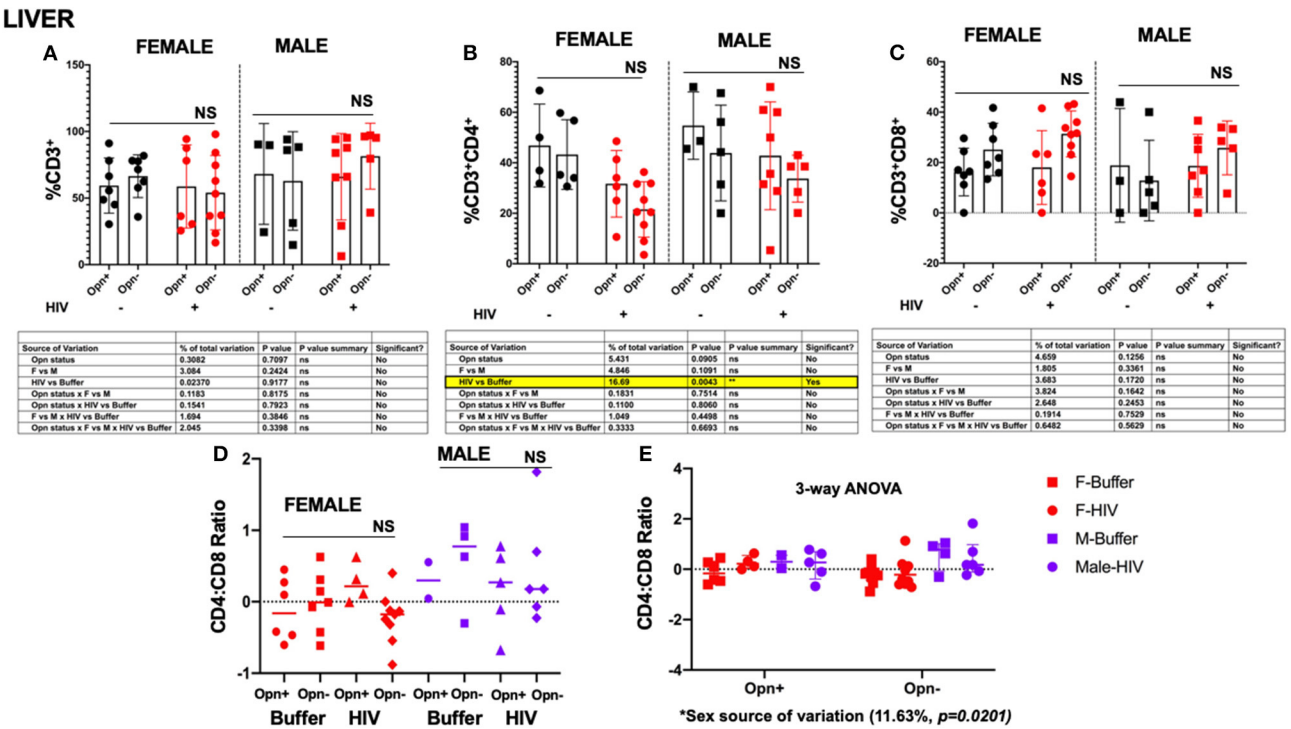

Source of Variation	% of total variation	P value	P value summary	Significant?
Opn status	0.3082	0.7097	ns	No
F vs M	3.084	0.2424	ns	No
HIV vs Buffer	0.02370	0.9177	ns	No
Opn status x F vs M	0.1183	0.8175	ns	No
Opn status x HIV vs Buffer	0.1541	0.7923	ns	No
F vs M x HIV vs Buffer	1.694	0.3846	ns	No
Opn status x F vs M x HIV vs Buffer	2.045	0.3398	ns	No

Source of Variation	% of total variation	P value	P value summary	Significant?
Opn status	5.431	0.0905	ns	No
F vs M	4.846	0.1091	ns	No
HIV vs Buffer	16.69	0.0043	**	Yes
Opn status x F vs M	0.1831	0.7514	ns	No
Opn status x HIV vs Buffer	0.1100	0.8060	ns	No
F vs M x HIV vs Buffer	1.049	0.4498	ns	No
Opn status x F vs M x HIV vs Buffer	0.3333	0.6693	ns	No

Source of Variation	% of total variation	P value	P value summary	Significant?
Opn status	4.659	0.1256	ns	No
F vs M	1.805	0.3361	ns	No
HIV vs Buffer	3.683	0.1720	ns	No
Opn status x F vs M	3.824	0.1642	ns	No
Opn status x HIV vs Buffer	2.648	0.2453	ns	No
F vs M x HIV vs Buffer	0.1914	0.7529	ns	No
Opn status x F vs M x HIV vs Buffer	0.6482	0.5629	ns	No

FIGURE 7 | Flow cytometric analyses of T cell subsets in the liver. **(A)** Shows the percentage of CD3+, **(B)** percentage of CD4+, and **(C)** percentage of CD8+. Individual points and mean ± SD are displayed. Three-way ANOVA, with Tukey's *post-hoc* for normally distributed data to determine the variation in the immune cells due to Opn status, sex differences, and infection; results are displayed below the bar charts with significant results highlighted. **(D,E)** CD4:CD8 ratio analyses were performed with three-way ANOVA for non-parametric continuous data and *post-hoc* test by Kruskal-Wallis to determine the immune cells' variation due to Opn status, sex differences, and infection. Three-way ANOVA for non-parametric continuous data and *post-hoc* test by Kruskal-Wallis to determine the variation in CD14 count due to Opn status, sex differences, and infection. Mean, and IQR are displayed in the graph. **Infected**: F-HIV-Opn+ $n = 6$, F-HIV-Opn– $n = 9$, M-HIV-Opn+ $n = 8$ and M-HIV-Opn– $n = 5$. **Uninfected**: F-Opn+ $n = 7$, F-Opn– $n = 7$, M-Opn+ $n = 3$ and M-Opn– $n = 5$.

differentially reduced in the absence of OPN expression. Two-way ANOVA between cell types (T cell, B cell, and monocytes) and OPN status revealed highly significant differences in the percent of leukocytes in tissues where OPN expression was unaffected or knockdown with aptamers (**Figures 10A,B**, Opn status, $P < 0.0001$). Surprisingly, comparing the two HIV-infected female groups in the spleen (**Figure 10A**, F-Opn+ 11.2 ± 6.9, F-Opn– 27.8 ± 13.8) and lung (**Figure 10A**, F-Opn+ 22.3 ± 6.5, F-Opn– 37.6 ± 22.2), with inhibition of OPN expression, there was an increase in percent frequency of T cells. This was also observed in lung (**Figure 10A**, M-Opn+ 39.84 ± 24.64, M-Opn– 59.5 ± 26.36) and liver (**Figure 10A**, M-Opn+ 66.02 ± 32.42, M-Opn– 81.46 ± 24.76) of infected males with reduced levels of OPN. Therefore, T cell infiltration was increased in infected mice with reduced OPN expression and likely contributed to the HIV-1 vRNA detected in these tissues (**Figures 3B**, **4B**). There was a decrease in the percent frequency of splenic B cells (**Figure 10A**, F-Opn+ 42.17 ± 32.73, F-Opn– 19.71 ± 19.25) and lungs (**Figure 10A**, F-Opn+ 20.78 ± 15.68, F-Opn– 7.26 ± 4.79) of HIV infected females with reduced OPN and the lung (**Figure 10A**, M-Opn+ 12.62 ± 5.441, M-Opn– 6.938 ± 3.25) and liver (**Figure 10A**, M-Opn+ 20.77 ± 10.34, M-Opn– 9.048 ± 10.33) of infected males with low OPN expression. Therefore, decreased OPN expression limited the recruitment of B cells into these tissues. An additional significant interaction between different immune cell types and OPN status was detected in the spleen (**Figure 10B**, $P = 0.0137$). These results collectively shed light on how the percent frequency of one cell type in a tissue and OPN expression might influence that of other leukocytes in a secondary lymphoid organ.

DISCUSSION

Replication-competent HIV-1 can persist within immune cells contained in secondary lymphoid tissues and other organs (43). Most recent estimates suggest that more than 70 years of uninterrupted ART is required to eliminate such reservoirs (4). Many factors affect the pharmacodynamics/kinetics of ART therapeutic efficacy (44–47). Therefore, understanding and identifying host proteins and associated cellular pathways that support viral persistence in tissues can inform therapeutic development aimed at halting HIV-1 spread and associated disease sequelae. This study shows evidence of osteopontin's (OPN) potential to affect the formation of HIV-infected tissue sanctuaries in female humanized mice. OPN expression is

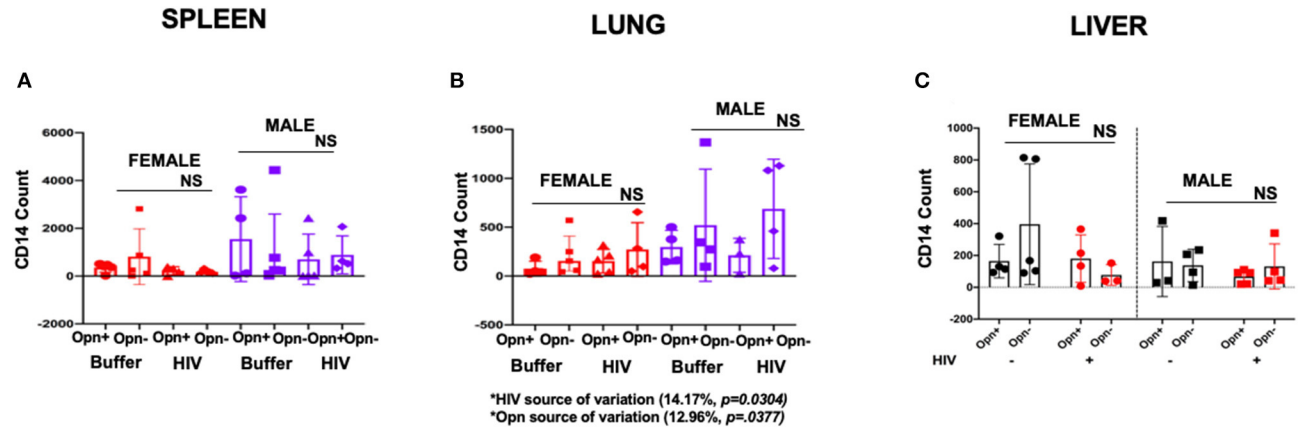

FIGURE 8 | Flow cytometric analyses of monocyte in the spleen **(A)**, lung **(B)**, and liver **(C)**. Three-way ANOVA for non-parametric continuous data and *post-hoc* test by Kruskal-Wallis to determine the variation in CD14 count in the spleen due to Opn status, sex differences, and infection. For spleen and lung the mean, and IQR are displayed in the graphs. For liver individual points and mean ± SD are displayed. Three-way ANOVA results to determine the variation in CD14 count in the liver due to Opn status, sex differences, and infection are displayed below the bar charts with significant results highlighted. **SPLEEN**_Infected: F-HIV-Opn+ $n = 4$, F-HIV-Opn– $n = 5$, M-HIV-Opn+ $n = 5$ and M-HIV-Opn– $n = 4$. Uninfected: F-Opn+ $n = 5$, F-Opn– $n = 5$, M-Opn+ $n = 4$ and M-Opn– $n = 4$. **LUNG**_Infected: F-HIV-Opn+ $n = 4$, F-HIV-Opn– $n = 5$, M-HIV-Opn+ $n = 5$ and M-HIV-Opn– $n = 4$. Uninfected: F-Opn+ $n = 4$, F-Opn– $n = 4$, M-Opn+ $n = 3$ and M-Opn– $n = 4$. $^{*}P < 0.05$, $^{**}P < 0.01$, $^{***}P < 0.001$, and $^{****}P < 0.0001$. **LIVER**_Infected: F-HIV-Opn+ $n = 4$, F-HIV-Opn– $n = 3$, M-HIV-Opn+ $n = 5$ and M-HIV-Opn– $n = 4$. Uninfected: F-Opn+ $n = 4$, F-Opn– $n = 5$, M-Opn+ $n = 3$ and M-Opn– $n = 4$.

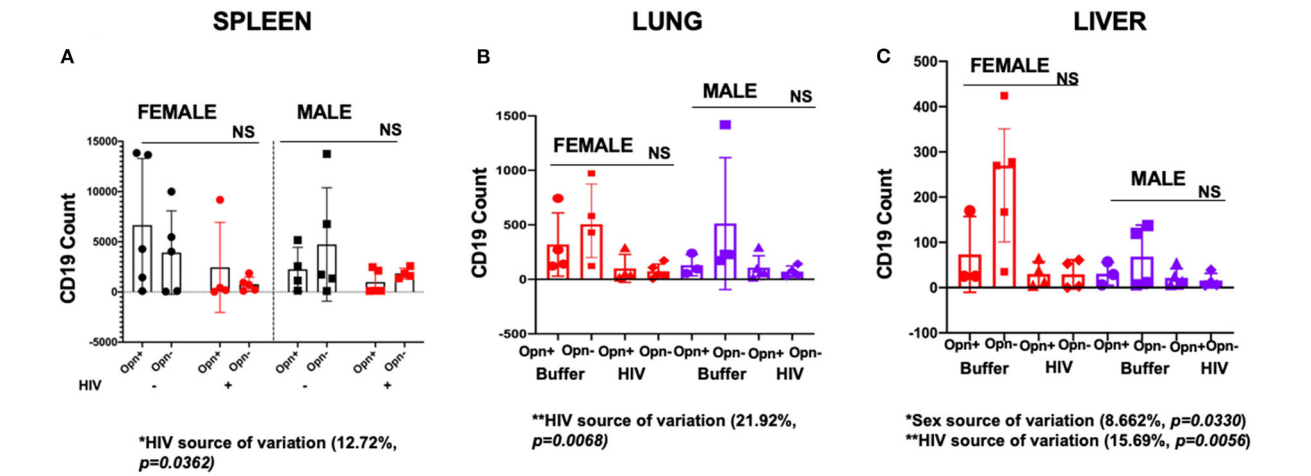

FIGURE 9 | Flow cytometric analyses of B cells in the spleen, lung, and liver. (**A**) Shows the cell counts of CD19 in the spleen, **(B)** lung and **(C)** liver. For Spleen individual points and mean±SD are displayed. Three-way ANOVA results to determine the variation in CD19 count in the spleen due to Opn status, sex differences, and infection are displayed below the bar charts with significant results highlighted. **SPLEEN**_Infected: F-HIV-Opn+ $n = 4$, F-HIV-Opn– $n = 5$, M-HIV-Opn+ $n = 5$ and M-HIV-Opn– $n = 4$. Uninfected: F-HIV-Opn+ $n = 5$, F-HIV-Opn– $n = 5$, M-HIV-Opn+ $n = 5$ and M-HIV-Opn– $n = 5$. For lung and liver, three-way ANOVA for non-parametric continuous data and *post-hoc* test by Kruskal-Wallis was used to determine the variation in CD19 count due to Opn status, sex differences, and infection. Mean and IQR are displayed in the graphs. **LUNG**_Infected: F-HIV-Opn+ $n = 4$, F-HIV-Opn– $n = 5$, M-HIV-Opn+ $n = 5$ and M-HIV-Opn– $n = 4$. Uninfected: F-HIV-Opn+ $n = 4$, F-HIV-Opn– $n = 4$, M-HIV-Opn+ $n = 3$ and M-HIV-Opn– $n = 4$. **LIVER**_Infected: F-HIV-Opn+ $n = 4$, F-HIV-Opn– $n = 4$, M-HIV-Opn+ $n = 5$ and M-HIV-Opn– $n = 4$. Uninfected: F-HIV-Opn+ $n = 3$, F-HIV-Opn– $n = 5$, M-HIV-Opn+ $n = 3$ and M-HIV-Opn– $n = 4$. $^{*}P < 0.05$, $^{**}P < 0.01$, $^{***}P < 0.001$, and $^{****}P < 0.0001$.

increased in the plasma and cerebrospinal fluid (CSF) in HIV-1 infection. Previous studies have implicated OPN in enhancing HIV-1 infection and acting as a chemoattractant to monocytes PMNs (16, 19, 20). Therefore, the decline in tissue persistence seen in this study could be related to reducing HIV replication, decreased trafficking of infected cells into the tissues, or a combination of the two. An essential consideration of the NSG-hCD34 model is to understand that the phenotypes observed are also likely in direct relationship to the genetic background of the donor cells used for engraftment and could explain some of the

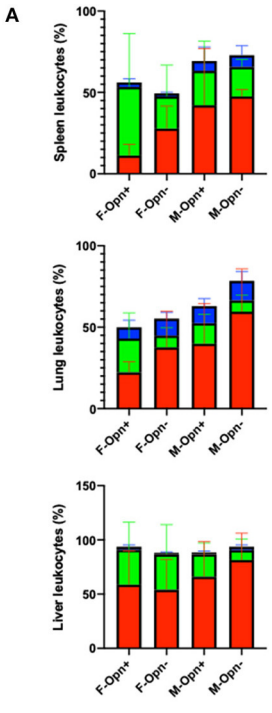

B

Source of Variation	% of total variation	P value	P value summary	Significant?
Interaction	16.13	0.0137	*	Yes
Cell types	2.131	0.5109	ns	No
Opn status	25.70	<0.0001	****	Yes

Source of Variation	% of total variation	P value	P value summary	Significant?
Interaction	10.40	0.0704	ns	No
Cell types	2.273	0.4412	ns	No
Opn status	41.69	<0.0001	****	Yes

Source of Variation	% of total variation	P value	P value summary	Significant?
Interaction	5.095	0.3246	ns	No
Cell types	0.06115	0.9934	ns	No
Opn status	60.81	<0.0001	****	Yes

FIGURE 10 | The proportion of T cells, B cells, and monocytes in the infected spleen, lung, and liver. **(A)** Shows stacked bar charts depicting the proportion of hCD3, hCD19, and hCD14 as a percentage of hCD45 in the different tissues assessed. Proportional differences were computed by two-way ANOVA, and the results are displayed in **(B)** with significant results highlighted. $^{*}P < 0.05$, $^{**}P < 0.01$, $^{***}P < 0.001$, and $^{****}P < 0.0001$.

variation observed in this study (33). Nevertheless, through 3-way ANOVA to further investigate the sources of variation and interaction, we found significant impacts of HIV, sex, and OPN.

Infected female mice in which OPN expression was blocked, had lower viral persistence in the spleen as evident by the significantly fewer number of viral RNA foci detected. The spleen, a secondary lymphoid organ, is a major HIV sanctuary with HIV infected T cells found in the white pulp and macrophages in the red pulp. In this study, most of the vRNA foci in the spleen were localized to the white pulp. In a humanized mouse model with ART beginning 4 weeks post-infection and continuing for a total time of 22 weeks, HIV viral DNA decreased 2-logs and remained stable highlighting the limitations of ART to hasten the turnover of infected cells in the spleen (48). Splenic T cell dysfunction has been previously associated with a decrease CD4 T cells and concomitant increase in CD8 cytotoxic lymphocytes (49). Our results indicated a similar trend of low CD4 and increased CD8, which was not recovered by inhibiting OPN expression. There were no significant differences in CD4 or CD8 levels with OPN expression, suggesting that OPN does not modulate these cells' recruitment into the spleen. Rather, reduced OPN expression results in a decline in HIV replication and lower vRNA persistence in tissues. Therefore, while infected T cells can extravasate into the spleen in animals with reduced OPN, HIV replication in these cells is limited. Female infected mice suffered a more significant loss in splenic CD4 than males. This likely reflects reported sex differences in HIV pathogenesis with infected females showing a faster rate of CD4 cell loss than males (11).

B-cell follicles found in lymph nodes and gut-associated lymphoid tissue are sites of dynamic interaction between specific T-cell subsets and NK cells involved in immunity against HIV (50, 51). We also evaluated whether HIV-mediated B cell loss can be recovered by lowering viral persistence in the spleen. We found, however, that B cells declined in all infected animals irrespective of OPN levels. Interestingly, a role for OPN in B-cell differentiation in immune-mediated inflammatory disorders, including multiple sclerosis, alcoholic and non-alcoholic liver diseases, and others, has been reported (52, 53). This could potentially explain why CD19 numbers did not increase in the HIV-infected groups with reduced OPN expression.

In HIV infection, monocyte recruitment is increased contributing to tissue macrophage viral reservoirs (49, 54). However, in this low-level chronic infection model, we did not observe an increase in monocyte recruitment into the spleen. Rather in HIV-infected animals with or without OPN, CD14 cells were decreased. Further characterization of monocytic subsets with CD16, chemokine profiling, and sampling at an earlier time point would shed further light on their movement from blood to tissues.

Analysis of lungs also revealed a decrease in viral persistence in infected females with reduced OPN levels. Like the spleen, we did not observe CD4 or B cell recovery or CD8 decrease in the lungs despite the lower levels of HIV vRNA seen in

this tissue. The prevalence of lung complications is increased with HIV infection and include respiratory infections like Mycobacterium tuberculosis and non-infectious dysfunctions such as emphysema and chronic obstructive pulmonary disease (55). These complications have been attributed to increased CD8 infiltrates in lung mucosa (55). Therefore, although reducing OPN expression lowered virus replication levels in the lungs, immune dysfunction was not reversed. With HIV infection monocyte levels were decreased in the lungs but interestingly, mice with reduced OPN expression showed a trend of an increased number of monocytes compared to animals with normal levels of OPN, however the sample sizes were small.

Sex differences in HIV persistence were observed in the liver. Males with and without OPN exhibited higher levels of viral RNA than females, and three out of seven males had giant hCD45$^+$ clusters of cells that produced viral RNA. This pattern was not observed in females, even those with higher levels of virus in plasma. Reduction of OPN in females resulted in lower viral RNA in the liver but not in male mice, and T cell dysfunction and B cell decline again were not recovered in this context. Overall, in all tissues assessed, inhibition of OPN expression resulted in greater recruitment of CD3$^+$ T cells and a lower influx of B cells.

Collectively, our findings demonstrate the potential for host factors to influence in a sex-dependent or -independent manner immune cell-HIV replication dynamics in tissues and warrant further investigation of the mechanisms involved.

DATA AVAILABILITY STATEMENT

The original contributions presented in the study are included in the article/**Supplementary Materials**, further inquiries can be directed to the corresponding author/s.

ETHICS STATEMENT

The animal study was reviewed and approved by Johns Hopkins University Animal Care and Use Committee and Institutional Review Board (Protocol # MO17M12).

AUTHOR CONTRIBUTIONS

AB and FM designed the study. FM, EG, TB, and AB performed the mouse studies. KM, CL, and BC co-designed and assisted with necropsy strategy. AB prepared tissue samples. FM collected flow data and conducted analyses. FM and AB performed data analyses and wrote manuscript. All authors contributed to the article and approved the submitted version.

FUNDING

This work was supported by the National Institutes of Health, National Institutes of Neurological Disorders and Stroke, R01NS102006 to AB.

ACKNOWLEDGMENTS

The authors would like to thank Peter Calabresi for access to the MACsquant Analyzer 10, Matthew Smith, and Justin Glenn for training on this cytometer and sharing their protocols and best practices for FACS analyses of cell suspensions generated from tissues.

SUPPLEMENTARY MATERIAL

The Supplementary Material for this article can be found online at: https://www.frontiersin.org/articles/10.3389/fviro.2021.690360/full#supplementary-material

Supplementary Figure 1 | Gating strategy for spleen tissue. **(A)** Shows identification of single cells, forward (FSC) vs. side-scatter (SSC), and gating for human CD45, CD3 and CD8 cells. **(B)** Representative dot plots and histograms of hCD4 vs hCD8 on female and male tissue experimental groups.

Supplementary Figure 2 | Gating strategy for lung tissue. **(A)** Shows identification of single cells, forward (FSC) vs. side-scatter (SSC), and gating for human CD45, CD3 and CD8 cells. **(B)** Representative dot plots and histograms of hCD4 vs. hCD8 on female and male tissue experimental groups.

Supplementary Figure 3 | Gating strategy for liver tissue. **(A)** Shows identification of single cells, forward (FSC) vs. side-scatter (SSC), and gating for human CD45, CD3 and CD8 cells. **(B)** Representative dot plots and histograms of hCD4 vs. hCD8 on female and male tissue experimental groups.

Supplementary Figure 4 | Gating strategy for monocytes from spleen, lung and liver tissue. **(A,D,G)** Shows identification of single cells, forward vs. side-scatter, and gating for human CD45 and CD14. **(B,C)**, **(E,F)**, and **(H,I)** Representative contour plots hCD14 vs side scatter (SSC) on female and male tissue experimental groups.

Supplementary Figure 5 | Gating strategy for B-cells from spleen and lung tissue. **(A)** Shows identification of single cells, forward vs. side-scatter, and gating for human CD45 and CD19. **(B)** Representative contour plots hCD19 vs. side scatter (SSC) on female and male tissue experimental groups.

Supplementary Figure 6 | Gating strategy for B-cells from liver tissue. **(A)** Shows identification of single cells, forward vs. side-scatter, and gating for human CD45 and CD19. **(B)** Representative contour plots hCD19 vs side scatter (SSC) on female and male tissue experimental groups.

REFERENCES

1. Chaillon A, Gianella S, Dellicour S, Rawlings SA, Schlub TE, De Oliveira MF, et al. HIV persists throughout deep tissues with repopulation from multiple anatomical sources. *J Clin Invest*. (2020) 130:1699–712. doi: 10.1172/JCI134815
2. Wong JK, Hezareh M, Günthard HF, Havlir DV, Ignacio CC, Spina CA, et al. Recovery of replication-competent HIV despite prolonged suppression of plasma viremia. *Science*. (1997) 278:1291–5. doi: 10.1126/science.278.5341.1291
3. Yukl SA, Shergill AK, Ho T, Killian M, Girling V, Epling L, et al. The distribution of HIV DNA and RNA in cell subsets differs in gut and blood of HIV-positive patients on ART: implications for viral persistence. *J Infect Dis*. (2013) 208:1212–20. doi: 10.1093/infdis/jit308
4. Nixon CC, Mavigner M, Sampey GC, Brooks AD, Spagnuolo RA, Irlbeck DM, et al. Systemic HIV and SIV latency reversal via non-canonical NF-kappaB signalling *in vivo*. *Nature*. (2020) 578:160–5. doi: 10.1038/s41586-020-1951-3
5. Espinosa-Garcia C, Aguilar-Hernandez A, Cervantes M, Morali G. Effects of progesterone on neurite growth inhibitors in the

hippocampus following global cerebral ischemia. *Brain Res*. (2014) 1545:23–34. doi: 10.1016/j.brainres.2013.11.030
6. Darcis G, Berkhout B, Pasternak AO. The quest for cellular markers of HIV reservoirs: any color you like. *Front Immunol*. (2019) 10:2251. doi: 10.3389/fimmu.2019.02251
7. Alexaki A, Liu Y, Wigdahl B. Cellular reservoirs of HIV-1 and their role in viral persistence. *Curr HIV Res*. (2008) 6:388–400. doi: 10.2174/157016208785861195
8. Griesbeck M, Scully E, Altfeld M. Sex and gender differences in HIV-1 infection. *Clin Sci*. (2016) 130:1435–51. doi: 10.1042/CS20160112
9. Johnston RE, Heitzeg MM. Sex, age, race and intervention type in clinical studies of HIV cure: a systematic review. *AIDS Res Hum Retroviruses*. (2015) 31:85–97. doi: 10.1089/aid.2014.0205
10. Sterling TR, Lyles CM, Vlahov D, Astemborski J, Margolick JB, Quinn TC. Sex differences in longitudinal human immunodeficiency virus type 1 RNA levels among seroconverters. *J Infect Dis*. (1999) 180:666–72. doi: 10.1086/314967
11. El-Badry E, Macharia G, Claiborne D, Brooks K, Dilernia DA, Goepfert P, et al. Better viral control despite higher CD4(+) T cell activation during acute HIV-1 infection in Zambian women is linked to the sex hormone estradiol. *J Virol*. (2020) 94:JVI.00758-20. doi: 10.1128/JVI.00758-20
12. Chow FC, Regan S, Zanni MV, Looby SE, Bushnell CD, Meigs JB, et al. Elevated ischemic stroke risk among women living with HIV infection. *AIDS*. (2018) 32:59–67. doi: 10.1097/QAD.0000000000001650
13. Raghavan A, Rimmelin DE, Fitch KV, Zanni MV. Sex differences in select non-communicable HIV-associated comorbidities: exploring the role of systemic immune activation/inflammation. *Curr HIV AIDS Rep*. (2017) 14:220–8. doi: 10.1007/s11904-017-0366-8
14. Scully EP. Sex differences in HIV infection. *Curr HIV AIDS Rep*. (2018) 15:136–46. doi: 10.1007/s11904-018-0383-2
15. Massanella M, Fromentin R, Chomont N. Residual inflammation and viral reservoirs: alliance against an HIV cure. *Curr Opin HIV AIDS*. (2016) 11:234–41. doi: 10.1097/COH.0000000000000230
16. Burdo TH, Ellis RJ, Fox HS. Osteopontin is increased in HIV-associated dementia. *J Infect Dis*. (2008) 198:715–22. doi: 10.1086/590504
17. Lin YH, Yang-Yen HF. The osteopontin-CD44 survival signal involves actication of the phosphatidylinositol 3-kinase/Adt signaling pathway. *J Biol Chem*. (2001) 276:46024–30. doi: 10.1074/jbc.M105132200
18. Geissinger E, Weisser C, Fischer P, Schartl M, Wellbrock C. Autocrine stimulation by osteopontin contributes to antiapoptotic signalling of melanocytes in dermal collagen. *Cancer Res*. (2002) 62:4820–8. Available online at: https://cancerres.aacrjournals.org/content/62/16/4820.long
19. Brown A, Islam T, Adams R, Nerle S, Kamara M, Eger C, et al. Osteopontin enhances HIV replication and is increased in the brain and cerebrospinal fluid of HIV-infected individuals. *J Neurovirol*. (2011) 17:382–92. doi: 10.1007/s13365-011-0035-4
20. Burdo TH, Wood MR, Fox HS. Osteopontin prevents monocyte recirculation and apoptosis. *J Leukoc Biol*. (2007) 81:1504–11. doi: 10.1189/jlb.1106711
21. Lund SA, Wilson CL, Raines EW, Tang J, Giachelli CM, Scatena M. Osteopontin mediates macrophage chemotaxis via α4 and α9 integrins and survival via the α4 integrin. *J Cell Biochem*. (2013) 114:1194–202. doi: 10.1002/jcb.24462
22. Wei J, Marisetty A, Schrand B, Gabrusiewicz K, Hashimoto Y, Ott M, et al. Osteopontin mediates glioblastoma-associated macrophage infiltration and is a potential therapeutic target. *J Clin Invest*. (2019) 129:137–49. doi: 10.1172/JCI121266
23. Gorantla S, Makarov E, Finke-Dwyer J, Castanedo A, Holguin A, Gebhart CL, et al. Links between progressive HIV-1 infection of humanized mice and viral neuropathogenesis. *Am J Pathol*. (2010) 177:2938–49. doi: 10.2353/ajpath.2010.100536
24. Mi Z, Guo H, Russell MB, Liu Y, Sullenger BA, Kuo PC. RNA aptamer blockade of osteopontin inhibits growth and metastasis of MDA-MB231 breast cancer cells. *Mol Ther*. (2009) 17:153–61. doi: 10.1038/mt.2008.235
25. Kardava L, Moir S, Wang W, Ho J, Buckner CM, Posada JG, et al. Attenuation of HIV-associated human B cell exhaustion by siRNA downregulation of inhibitory receptors. *J Clin Invest*. (2011) 121:2614–24. doi: 10.1172/JCI45685
26. Moir S, Buckner CM, Ho J, Wang W, Chen J, Waldner AJ, et al. B cells in early and chronic HIV infection: evidence for preservation of immune function associated with early initiation of antiretroviral therapy. *Blood*. (2010) 116:5571–9. doi: 10.1182/blood-2010-05-285528
27. Serrano-Villar S, Moreno S, Fuentes-Ferrer M, Sanchez-Marcos C, Avila M, Sainz T, et al. The CD4:CD8 ratio is associated with markers of age-associated disease in virally suppressed HIV-infected patients with immunological recovery. *HIV Med*. (2014) 15:40–9. doi: 10.1111/hiv.12081
28. Barnett D, Walker B, Landay A, Denny TN. CD4 immunophenotyping in HIV infection. *Nat Rev Microbiol*. (2008) 6(11 Suppl.):S7–15. doi: 10.1038/nrmicro1998
29. Mahmud FJ, Du Y, Greif E, Boucher T, Dannals RF, Mathews WB, et al. Osteopontin/secreted phosphoprotein-1 behaves as a molecular brake regulating the neuroinflammatory response to chronic viral infection. *J Neuroinflamm*. (2020) 17:273. doi: 10.1186/s12974-020-02002-0
30. Monaco G, Chen H, Poidinger M, Chen J, de Magalhaes JP, Larbi A. flowAI: automatic and interactive anomaly discerning tools for flow cytometry data. *Bioinformatics*. (2016) 32:2473–80. doi: 10.1093/bioinformatics/btw191
31. Su H, Cheng Y, Sravanam S, Mathews S, Gorantla S, Poluektova LY, et al. Immune activations and viral tissue compartmentalization during progressive HIV-1 infection of humanized mice. *Front Immunol*. (2019) 10:340. doi: 10.3389/fimmu.2019.00340
32. Vanwolleghem T, Libbrecht L, Hansen BE, Desombere I, Roskams T, Meuleman P, et al. Factors determining successful engraftment of hepatocytes and susceptibility to hepatitis B and C virus infection in uPA-SCID mice. *J Hepatol*. (2010) 53:468–76. doi: 10.1016/j.jhep.2010.03.024
33. Allen TM, Brehm MA, Bridges S, Ferguson S, Kumar P, Mirochnitchenko O, et al. Humanized immune system mouse models: progress, challenges and opportunities. *Nat Immunol*. (2019) 20:770–4. doi: 10.1038/s41590-019-0416-z
34. Araínga M, Edagwa B, Mosley RL, Poluektova LY, Gorantla S, Gendelman HE. A mature macrophage is a principal HIV-1 cellular reservoir in humanized mice after treatment with long acting antiretroviral therapy. *Retrovirology*. (2017) 14:17. doi: 10.1186/s12977-017-0344-7
35. Noto A, Procopio FA, Banga R, Suffiotti M, Corpataux JM, Cavassini M, et al. CD32(+) and PD-1(+) lymph node CD4 T cells support persistent HIV-1 transcription in treated aviremic individuals. *J Virol*. (2018) 92:e00901–18. doi: 10.1128/JVI.00901-18
36. Davy-Mendez T, Napravnik S, Zakharova O, Kuruc J, Gay C, Hicks CB, et al. Acute HIV infection and CD4/CD8 ratio normalization after antiretroviral therapy initiation. *J Acquir Immune Defic Syndr*. (2018) 79:510–8. doi: 10.1097/QAI.0000000000001843
37. Sauter R, Huang R, Ledergerber B, Battegay M, Bernasconi E, Cavassini M, et al. CD4/CD8 ratio and CD8 counts predict CD4 response in HIV-1-infected drug naive and in patients on cART. *Medicine*. (2016) 95:e5094. doi: 10.1097/MD.0000000000005094
38. Serrano-Villar S, Sainz T, Lee SA, Hunt PW, Sinclair E, Shacklett BL, et al. HIV-infected individuals with low CD4/CD8 ratio despite effective antiretroviral therapy exhibit altered T cell subsets, heightened CD8+ T cell activation, and increased risk of non-AIDS morbidity and mortality. *PLoS Pathogens*. (2014) 10:e1004078. doi: 10.1371/journal.ppat.1004078
39. Eger C, Cirelli K, Budiaman J, Brown A. Noncontiguous protein interaction domains in osteopontin contribute to enhance HIV-1 replication. *J Hum Virol Retrovirol*. (2014) 1:7–14. doi: 10.15406/jhvrv.2014.01.00003
40. Anas A, van der Poll T, de Vos AF. Role of CD14 in lung inflammation and infection. *Crit Care*. (2010) 14:209. doi: 10.1186/cc8850
41. Lee HK, Dunzendorfer S, Soldau K, Tobias PS. Double-stranded RNA-mediated TLR3 activation is enhanced by CD14. *Immunity*. (2006) 24:153–63. doi: 10.1016/j.immuni.2005.12.012
42. Moir S, Fauci AS. Nef, macrophages and B cells: a highway for evasion. *Immunol Cell Biol*. (2010) 88:1–2. doi: 10.1038/icb.2009.82
43. Marsden MD. Benefits and limitations of humanized mice in HIV persistence studies. *Retrovirology*. (2020) 17:7. doi: 10.1186/s12977-020-00516-2

44. Hendrix CW. The clinical pharmacology of antiretrovirals for HIV prevention. *Curr Opin HIV AIDS*. (2012) 7:498–504. doi: 10.1097/COH.0b013e32835847ae
45. Dionne B. Key Principles of antiretroviral pharmacology. *Infect Dis Clin North Am*. (2019) 33:787–805. doi: 10.1016/j.idc.2019.05.006
46. Marx A, Alian A. The road less traveled: HIV's use of alternative routes through cellular pathways. *J Virol*. (2015) 89:5204–12. doi: 10.1128/JVI.03684-14
47. Goff SP. Host factors exploited by retroviruses. *Nat Rev Microbiol*. (2007) 5:253–63. doi: 10.1038/nrmicro1541
48. Rochat MA, Schlaepfer E, Kuster SP, Li D, Audige A, Ivic S, et al. Monitoring HIV DNA and cellular activation markers in HIV-infected humanized mice under cART. *Virol J*. (2018) 15:191. doi: 10.1186/s12985-018-1101-9
49. Williams DW, Engle EL, Shirk EN, Queen SE, Gama L, Mankowski JL, et al. Splenic damage during SIV infection: role of T-cell depletion and macrophage polarization and infection. *Am J Pathol*. (2016) 186:2068–87. doi: 10.1016/j.ajpath.2016.03.019
50. Bronnimann MP, Skinner PJ, Connick E. The B-cell follicle in HIV infection: barrier to a cure. *Front Immunol*. (2018) 9:20. doi: 10.3389/fimmu.2018.00020
51. Connick E, Folkvord JM, Lind KT, Rakasz EG, Miles B, Wilson NA, et al. Compartmentalization of simian immunodeficiency virus replication within secondary lymphoid tissues of rhesus macaques is linked to disease stage and inversely related to localization of virus-specific CTL. *J Immunol*. (2014) 193:5613–25. doi: 10.4049/jimmunol.1401161
52. Tahir S, Fukushima Y, Sakamoto K, Sato K, Fujita H, Inoue J, et al. A CD153+CD4+ T follicular cell population with cell-senescence features plays a crucial role in lupus pathogenesis via osteopontin production. *J Immunol*. (2015) 194:5725–35. doi: 10.4049/jimmunol.1500319
53. Rittling SR, Singh R. Osteopontin in immune-mediated diseases. *J Dent Res*. (2015) 94:1638–45. doi: 10.1177/0022034515605270
54. Fischer T, Wyatt CM, D'Agati VD, Croul S, McCourt L, Morgello S, et al. Mononuclear phagocyte accumulation in visceral tissue in HIV encephalitis: evidence for increased monocyte/macrophage trafficking and altered differentiation. *Curr HIV Res*. (2014) 12:201–12. doi: 10.2174/1570162X12666140713165141
55. Muema DM, Mthembu M, Schiff AE, Singh U, Corleis B, Chen D, et al. Contrasting inflammatory signatures in peripheral blood and bronchoalveolar cells reveal compartment-specific effects of HIV infection. *Front Immunol*. (2020) 11:864. doi: 10.3389/fimmu.2020.00864

Conflict of Interest: The authors declare that the research was conducted in the absence of any commercial or financial relationships that could be construed as a potential conflict of interest.

Publisher's Note: All claims expressed in this article are solely those of the authors and do not necessarily represent those of their affiliated organizations, or those of the publisher, the editors and the reviewers. Any product that may be evaluated in this article, or claim that may be made by its manufacturer, is not guaranteed or endorsed by the publisher.